Epithelia-sensory neuron crosstalk underlies cholestatic itch induced by lysophosphatidylcholine

Yong Chen, Zi-Long Wang, Michele Yeo, Qiao-Juan Zhang, Ana E. López-Romero, Hui-Ping Ding, Xin Zhang, Qian Zeng, Sara L. Morales-Lázaro, Carlene Moore, Ying-Ai Jin, Huang-He Yang, Johannes Morstein, Andrey Bortsov, Marcin Krawczyk, Frank Lammert, Manal Abdelmalek, Anna Mae Diehl, Piotr Milkiewicz, Andreas E. Kremer, Jennifer Y. Zhang, Andrea Nackley, Tony E. Reeves, Mei-Chuan Ko, Ru-Rong Ji, Tamara Rosenbaum, Wolfgang Liedtke

PII: S0016-5085(21)00576-X
DOI: https://doi.org/10.1053/j.gastro.2021.03.049
Reference: YGAST 64241

To appear in: *Gastroenterology*
Accepted Date: 22 March 2021

Please cite this article as: Chen Y, Wang Z-L, Yeo M, Zhang Q-J, López-Romero AE, Ding H-P, Zhang X, Zeng Q, Morales-Lázaro SL, Moore C, Jin Y-A, Yang H-H, Morstein J, Bortsov A, Krawczyk M, Lammert F, Abdelmalek M, Diehl AM, Milkiewicz P, Kremer AE, Zhang JY, Nackley A, Reeves TE, Ko M-C, Ji R-R, Rosenbaum T, Liedtke W, Epithelia-sensory neuron crosstalk underlies cholestatic itch induced by lysophosphatidylcholine, *Gastroenterology* (2021), doi: https://doi.org/10.1053/j.gastro.2021.03.049.

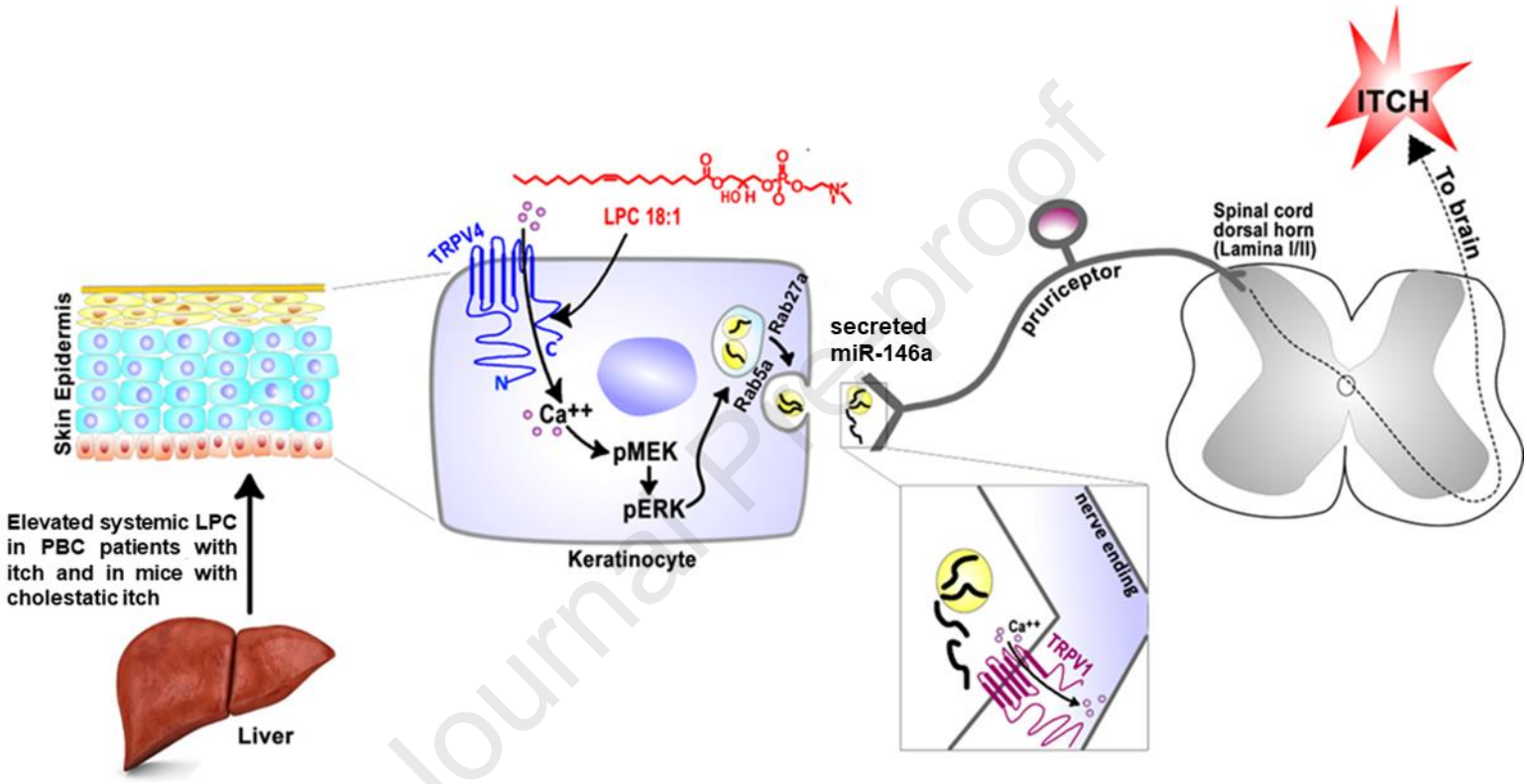

Epithelia-sensory neuron crosstalk underlies cholestatic itch induced by lysophosphatidylcholine

Short title: Lysophosphatidylcholine in cholestatic itch

Yong Chen[1*†], Zi-Long Wang[1, 2*], Michele Yeo[1], Qiao-Juan Zhang[1], Ana E. López-Romero[3], Hui-Ping Ding[4], Xin Zhang[2], Qian Zeng[1], Sara L. Morales-Lázaro[3], Carlene Moore[1], Ying-Ai Jin[5], Huang-He Yang[6, 14], Johannes Morstein[7], Andrey Bortsov[2], Marcin Krawczyk[8, 9], Frank Lammert[9], Manal Abdelmalek[10], Anna Mae Diehl[10], Piotr Milkiewicz[8, 11], Andreas E. Kremer[12], Jennifer Y. Zhang[5], Andrea Nackley[2], Tony E. Reeves[13], Mei-Chuan Ko[4], Ru-Rong Ji[2, 14], Tamara Rosenbaum[3], Wolfgang Liedtke[1, 2, 14, 15, 16†]

[1]Department of Neurology, Duke University, Durham, NC 27710, USA

[2]Department of Anesthesiology, Duke University, Durham, NC 27710, USA

[3]Departamento de Neurociencia Cognitiva, Instituto de Fisiología Celular, Universidad Nacional Autónoma de México, Coyoacan, Mexico City, Mexico

[4]Department of Physiology and Pharmacology, Wake Forest University, Winston-Salem, NC 27157, USA

[5]Department of Dermatology, Duke University, Durham, NC 27710, USA

[6]Department of Biochemistry, Duke University, Durham, NC 27710, USA

[7]Department of Chemistry, New York University, New York, NY 10003, USA

[8]Liver and Internal Medicine Unit, Department of General, Transplant and Liver Surgery, Medical University of Warsaw, Warsaw 02-097, Poland

[9]Department of Medicine II, Saarland University Medical Center, Saarland University, Homburg 66421, Germany

[10]Division of Gastroenterology, Department of Medicine, Duke University, Durham, NC 27710, USA

[11]Translation Medicine Group, Pomeranian Medical University, Szczecin 70-204, Poland

[12]Department of Medicine 1, Gastroenterology, Hepatology, Pneumology and Endocrinology, Friedrich-Alexander-University Erlangen-Nürnberg, Erlangen D-91054, Germany

[13]Department of Molecular Medicine, Wake Forest University, Winston-Salem, NC 27157, USA

[14]Department of Neurobiology, Duke University, Durham, NC 27710, USA

[15]Neurology Clinics for Headache, Head-Pain and Trigeminal Sensory Disorders, Duke University, Durham NC 27705, USA

[16]Clinics for Innovative Pain Therapy, Department of Anesthesiology, Duke University, Raleigh NC 27512, USA

[*]=equally contributed 1st author

Grant Support:

This work was supported by National Institutes of Health Grant DE018549 and support from the Michael Ross Haffner Foundation (Charlotte, NC) to WL, NIH grants K12DE022793 and R01DE027454 to YC, grants Dirección General de Asuntos del Personal Académico (DGAPA)-Programa de Apoyo a Proyectos de Investigación e Innovación Tecnológica (PAPIIT) IN200720; Consejo Nacional de Ciencia y Tecnología (CONACyT) A1-S-8760 and Secretaría de Educación, Ciencia, Tecnología e Innovación del Gobierno de la Ciudad de México SECTEI/208/2019 to T.R.

Abbreviations used:

LPA, lysophosphatidic acid; LPC, lysophosphatidylcholine; KC, keratinocyte; DRG, dorsal root ganglion; i.d., intradermal; i.t., intrathecal; MEK, mitogen-activated protein kinase; ERK, extracellular signal-regulated kinase; PBC, primary biliary cholangitis; ANIT, α-naphthyl-isothiocyanate; miR-146a: microRNA-146a

[†]**Correspondence**

Yong Chen: yong.chen@duke.edu; +1-919-6840093

Wolfgang Liedtke: wolfgang@neuro.duke.edu; +1-919-6840058

Department of Neurology, Duke University, Durham, NC 27710, USA

Disclosures

The authors declare that they have no conflicts of interest with the contents of this article.

Acknowledgement: We would like to thank Ms. Kelsey Reynolds and Brittany Kelly for their technical assistance with training of rhesus monkeys and data collection (Wake Forest Uni.), Itzel Llorente and Jesús Aldair Canul-Sánchez from Instituto de Fisiología Celular, UNAM for technical assistance in patch-clamp experiments and production of TRPV4 mutants. Authors Michele Yeo, Qiao-Juan Zhang, and Ana E. López-Romero contributed equally.

BACKGROUND & AIMS: Limited understanding of pruritus mechanisms in cholestatic liver diseases hinders development of anti-pruritic treatments. Previous studies implicated lysophosphatidic acid (LPA) as a potential mediator of cholestatic pruritus.

METHODS: Pruritogenicity of LPC, LPA's precursor, was examined in naïve mice, cholestatic mice, and nonhuman primates. LPC's pruritogenicity involving keratinocyte-TRPV4 was studied using genetic and pharmacological approaches, cultured keratinocytes, ion channel physiology and structural-computational modeling. Activation of pruriceptor-sensory neurons by microRNA-146a (miR-146a), secreted from keratinocytes, was identified by *in-vitro* and *ex-vivo* Ca^{2+}-imaging assays. Sera from primary biliary cholangitis (PBC) patients were used for measuring the levels of LPC and miR-146a.

RESULTS: LPC was robustly pruritic in mice. TRPV4 in skin keratinocytes was essential for LPC-induced itch and itch in mice with cholestasis. 3D-structural modeling, site-directed mutagenesis and channel function analysis suggested a TRPV4 C-terminal motif for LPC binding and channel activation. In keratinocytes, TRPV4-activation by LPC induced extracellular release of miR-146a, which activated $TRPV1^+$-sensory neurons to cause itch. Both LPC and miR-146a levels were elevated in sera of PBC patients with itch and correlated with itch intensity. Moreover, LPC and miR-146a were also increased in sera of cholestatic mice and elicited itch in nonhuman primates.

CONCLUSIONS: We identified LPC as a novel cholestatic pruritogen that induces itch through epithelia-sensory neuron crosstalk, whereby it directly activates skin keratinocyte-TRPV4, which rapidly release miR-146a to activate skin-innervating $TRPV1^+$-pruriceptor sensory neurons. Our findings support the new concept of the skin, as a sensory organ, playing a critical role in cholestatic itch, beyond liver, peripheral sensory neurons and central neural pathways supporting pruriception.

Keywords: Lysophosphatidylcholine; Cholestatic itch; Keratinocyte TRPV4; miR-146a; TRPV1 pruriceptor

Treatment for itch (pruritus) associated with chronic liver disease represents a severe unmet medical need.[1] Cholestatic itch is a debilitating symptom which has significant prevalence in patients with hepatobiliary diseases: namely primary biliary cholangitis (PBC), primary sclerosing cholangitis (PSC), and intrahepatic cholestasis of pregnancy (ICP).[1] Therapeutic recourse is dire because the underlying pathophysiology remains largely elusive. Cholestatic itch has been linked to bile acids, bilirubin, progesterone metabolites, and lysophosphatidic acid (LPA).[2-6] LPA is a bioactive phospholipid with diverse biological functions.[7] Autotaxin (ATX) catalyzes the hydrolysis of lysophosphatidylcholine (LPC) to LPA, and it has been demonstrated that levels of ATX and LPA correlate with itch intensity in patients with cholestatic liver disease[2]. In addition, a recent study suggested that LPA induces itch via TRPV1 and TRPA1.[8]

TRP ion channels have been implicated in the molecular mechanisms of itch, with experimental studies supporting significant roles for the chemo-irritant receptor TRPA1 and the heat-capsaicin receptor TRPV1 in primary sensory neurons, where both channels function not only in pain transduction, but also in pruriception.[9] TRPV4, a widely expressed multimodally-activated channel expressed in both innervated epithelia and sensory neurons, has also been found relevant for experimental itch.[9, 10] Our group has demonstrated a novel pro-pruritic role of TRPV4 in skin keratinocytes.[10]

LPC, the precursor of LPA, has been linked with a variety of diseases that are pruritic. For instance, previous studies demonstrated that LPC concentrations were increased in blood[11] and lesional skin[12] of psoriasis patients. Mass spectrometry of lesional skin from atopic dermatitis patients revealed an increase of short-chain LPC species.[13] Moreover, a recent study found that LPC concentrations were significantly elevated systemically in uremic patients with pruritus.[14] This evidence and the involvement of LPC's metabolite LPA in cholestatic itch prompted us to ask whether LPC could also contribute to cholestatic itch. We sought to address: (i) Does LPC induce itch? (ii) Does LPC-triggered itch involve TRPV4 in skin keratinocytes, given the pro-pruritic role of TRPV4 in these cells? (iii) Does direct crosstalk between skin keratinocytes and sensory neurons underlie LPC-induced itch? and (iv) Is LPC elevated systemically in cholestatic liver disease, both in experimental animals as well as patients with itch? Here we identified LPC

as a novel pruritogen that elicited robust scratching behaviors in mice and nonhuman primates. LPC functioned via TPRV4 activation in keratinocytes which we explain mechanistically in an LPC-TRPV4 binding model. Interestingly, this signaling in keratinocytes induced extracellular release of microRNA-146a (miR-146a), which rapidly activated $TRPV1^{+}$ pruriceptor sensory neurons to cause itch. Moreover, we found elevated levels of systemic LPC and miR-146a in PBC patients with itch and also in cholestatic mice. In cholestatic mice, we observed dependence of scratching behavior and systemic concentration of miR-146a on keratinocyte-TRPV4. Our findings suggest a hitherto underappreciated function of the epidermis and of TRPV4 in keratinocytes as key signaling molecule in cholestatic itch.

Materials and Methods

Additional details are provided in the Supplementary Materials.

Animals

Wild-type (WT, C57bl/6j), *Trpv1*-, *Trpa1*-, and *Tlr7*-knockout (KO) mice were from the Jackson Laboratory. *Trpv4*-KOs were generated in our laboratory.[10] Pirt-GCaMP3 mice, expressing the calcium indicator GCaMP3 in >96% of sensory neurons in the dorsal root ganglion (DRG), were from Dr. Xinzhong Dong.[15] Keratinocyte-specific, tamoxifen (tam)-inducible *Trpv4* KO (K14-Cre-ER^{tam}::$Trpv4^{lox/lox}$) mice were generated as previously described.[10] Sensory neuron-specific *Trpv4* KO (Nav1.8-Cre::$Trpv4^{lox/lox}$) were generated by mating $Trpv4^{fl/fl}$ mice with Nav1.8-Cre mice. The *Cre* mice enable gene recombination commencing at birth selectively in sensory neurons expressing Nav1.8. Mice with inducible expression of constitutively active B-raf (V600E) in keratinocytes were generated by crossing B-$raf^{CA/+}$ mice with K5-cre-ER^{tam} mice. All mouse lines have C57bl/6 background. Only male mice (2-3 months) were used for *in vivo* behavioral assays. Both male and female rhesus monkeys (*Macaca mulatta*, 11-18 years) were used for scratching behavior study. All animal protocols were approved by Institutional Animal Care and Use Committee (IACUC).

Human Subjects

Primary biliary cholangitis (PBC) patients were recruited at Warsaw Medical University, Poland and University Hospital of Erlangen, Germany. Itch intensity was quantified at the time-point of blood drawing using a visual analogue scale ranging from 0 to 10 (0-3: no/mild itch, 3-6: moderate itch, 6-10: severe/worst imaginable itch). Study protocols were approved by the local medical institutional review boards.

Behavioral Assessment

After intradermal (i.d.) injection of 50µl of chemical solutions into the mouse dorsal neck, scratching behavior was recorded and quantified as described in a blinded way.[10] To investigate the effects of the selective inhibitors on LPA-, LPC- or miR-146a-induced scratching behaviors, mice received an intraperitoneal (i.p.) injection of 0.25ml or an intrathecal (i.t., see approach below) injection of 5µl of inhibitor solutions 15min before pruritogen injections. To test whether LPC induces scratching behavior at the spinal cord level, 5µl of LPC was i.t. injected into the L4/L5 subarachnoid space. To examine whether i.d. injection of LPC or miR146a induces pain-like behavior, a mouse cheek model was used to differentiate itch from pain. To examine whether TRPV1-expressing sensory neurons contribute to LPC- or miR-146a-induced itch, we ablated the central terminals of TRPV1-expressing neurons by i.t. injection of 200ng resiniferatoxin (RTX).

Scratching behaviors in monkeys were performed as previously described.[16] 20µl of histamine, LPC or miR-146a solution was i.d. injected into the hindlimbs and the scratching behavior was recorded.

Mouse model of cholestasis was induced by α-naphthyl isothiocyanate (ANIT) administration via oral gavage for 5 days at 25mg/kg.[5] The scratching behavior was recorded for 1h before daily ANIT treatment.

In Vitro and Ex Vivo Ca^{2+} Imaging

Routine procedures were followed for Ca^{2+} imaging in cultured DRG neurons, keratinocytes, and HEK cells.[10] Ca^{2+} imaging was conducted after loading with Fura2-AM (Invitrogen). A previously established method was followed for *ex-vivo* Ca^{2+} imaging of DRG explants.[15] Intact DRGs (L4 or L5) were isolated

from naïve male or female Pirt-GCaMP3 mice. The explants were in pre-oxygenated ACSF and imaged using a Zeiss-780 upright confocal microscope (Carl Zeiss, Oberkochen, Germany). To investigate the effects of the inhibitors on LPA-, LPC-, or miR-146a-induced Ca^{2+} influx (as indicated in Figure legends), cells or DRGs were incubated with the inhibitors for 15 min before stimulation.

Electrophysiology

Currents were recorded using the inside-out configuration of the patch-clamp technique[17]. Single-channel recordings were carried out as described previously.[18]

Western Blot, Immunohistochemistry, and Quantitative Real-Time PCR

Experiments were performed according to the manufacturer's instructions and the standard procedures as previously described.[10]

Measurement of Released Vesicles and Extracellular miR-146a from Cultured Keratinocytes or Sera

Fifteen minutes after LPC stimulation, the supernatant of the cultured keratinocytes was harvested, followed by purification using a Vesicular Isolation kit (Invitrogen). Total RNA extraction was then carried out using a Total RNA Isolation kit (Invitrogen). For human PBC sera or sera from ANIT-treated mice, RNA was isolated using Qiagen miRNeasy Plasma/Serum kit. cDNA synthesis from extracted RNAs was performed and qPCR reactions for each sample were run in triplicates. To investigate the effects of the inhibitors on LPC-induced extracellular release of miR-146a (as indicated in Figure legends), cells were incubated with the inhibitors for 15min before stimulation.

Vesicular release from cultured keratinocytes was quantified by detecting acetylcholinesterase (AChE) activity in the extracellular release fluid.[19]

LPC Measurement in Sera and Skin

Blood and dorsal neck skin (~0.5x0.5cm) were harvested from ANIT- or control-treated mice at d5. Total levels of LPC were determined by an enzymatic colorimetric method.[20] Total level of LPC was detected at ~1mM in sera of control mice.

Serum levels of LPC in PBC patients were determined by the AbsoluteIDQ™ p180-kit (Biocrates, Life Sciences AG, Innsbruck, Austria). The assay allows simultaneous quantification of 188 metabolites, including 14 species of LPC. Total level of these LPC species was ~155µM in PBC patients without itch.

Statistical Analysis

All data are expressed as mean±SEM. Two tailed t-test and one-way or two-way ANOVA followed by Tukey's post-hoc test were used for group comparison (SPSS, version 25). For scratching behavior in nonhuman primates, analyses of repeated measures data were performed using a linear mixed model as implemented in SAS 9.4. The correlated nature of repeated measures was taken into account by using an autoregressive correlation matrix in the model specification. Between-group contrasts were evaluated for statistical significance using an F-statistic. Pearson's correlation coefficient and corresponding p value were calculated to assess the correlation between itch intensity and LPC and miR146a levels. $p<0.05$ indicated statistically significant differences.

Results

LPC Induces Itch via Keratinocyte-TRPV4

First, we addressed whether the known cholestatic pruritogen, LPA, induces pruritus via TRPV4. We found no evidence that LPA's pruritogenicity relies on TRPV4 (Figure.1*A*, Supplementary Figure.1).

Next we examined pruritogenicity of LPC, LPA's direct metabolic precursor. In mice, we observed dose-dependent scratching evoked by LPC (Figure.1*B*). LPC was robustly more potent than LPA, eliciting scratching, not pain-related wiping behavior (Figure.1*C*). Next we examined TRPV4-dependence of LPC-

induced scratching. Whereas WT and pan-null *Trpv4*-KO mice did not differ, mice treated systemically with TRPV4 inhibitors, GSK205 and HC067047, showed significantly reduced LPC-induced scratching (Figure.1*D*). We reasoned that findings of acute TRPV4 inhibition attenuating LPC-induced scratching suggest TRPV4-dependence, whereas the role of *Trpv4* was masked in pan-null *Trpv4*-KO mice likely because of gene-regulatory developmental compensation. To resolve this issue, we investigated LPC-induced scratching in *Trpv4* conditional knockout (cKO) mice. Tamoxifen-induced keratinocyte-*Trpv4* cKOs (K14-Cre-ER^{tam}::*Trpv4*$^{fl/fl}$) showed a >50% reduction, whereas sensory neuron-*Trpv4* cKOs (Nav1.8-Cre::*Trpv4*$^{fl/fl}$) did not differ to controls (Figure.1*D*). These findings indicate that skin keratinocyte-TRPV4, not sensory neuron-TRPV4, is needed for LPC-induced scratching. Different species of LPC induced robust scratching, with LPC(18:1) the most potent (Figure.1*E*). Moreover, LPC(18:1)-induced itch was also reduced in keratinocyte-*Trpv4* cKOs (Figure.1*F*). With clear-cut findings that i.d. LPC evokes robust scratching and relies on keratinocyte-*Trpv4*, we sought to elucidate whether selective LPC-stimulation of peripheral sensory neurons evokes sensory behaviors. We demonstrated that i.t. LPC did not elicit itch (Figure.1*G*), but long-lasting pain relying on sensory neuron-*Trpv4* (Supplementary Figure.2).These results suggest that LPC intradermally elicits itch via a non-neuronal peripheral mechanism critically involving keratinocyte-TRPV4, whereas LPC intrathecally relies on sensory neuron-TRPV4 to evoke pain.

Next, we tested whether the LPC→LPA-conversion contributes to LPC's pruritogenicity. If so, we expected the attenuated LPC-caused scratching in keratinocyte-*Trpv4* cKO mice to be suppressed further when inhibiting the LPC→LPA-conversion because no LPA is made while LPC's molecular target in keratinocytes, TRPV4, was selectively knocked-down. Using the selective autotaxin-inhibitor PF8380, we observed significant attenuation of residual LPC-induced scratching in keratinocyte-*Trpv4* cKOs. These findings suggest (i) the LPC→LPA conversion is relevant for scratching in-vivo, (ii) LPC, but not its "co-pruritogen" metabolite LPA, evokes scratching directly via keratinocyte-TRPV4 (Figure.1*H*), (iii) that residual itch is, at least partially, mediated via LPA and itch-relevant signaling of LPA to LPA-R5 and TRPV1 pruriceptor.[8]

We next determined whether LPC activatesTRPV4 in skin keratinocytes. We noticed that LPC, but not LPA, triggered Ca^{2+}-influx in cultured mouse and human keratinocytes in a TRPV4-dependent manner (Figure.1*I-P*).

We generated several relevant negative results (Supplementary Figures.3 and 4). LPC-induced Ca^{2+}-influx was independent of TRPV3, which is abundantly expressed in skin keratinocytes and known to contribute to itch.[21] In addition, LPC-induced itch was not significantly altered when inhibiting TRPV3, indicating the pruritogenic effects of LPC may not rely on TRPV3. Similar findings were recorded for mechanosensitive-channel Piezo1 in keratinocytes,[22] and for pruritogenic effects of Piezo1-activation using Yoda-1, which were independent of TRPV4.

LPC Activates TRPV4 Directly via a putative C-terminal Binding Pocket

We next tested whether LPC activates TRPV4 by direct binding to the channel. LPC(18:1), a major bioactive LPC sub-species, was selected because it is the most potent pruritogen (Figure.1*E*).

We first found there were no significant effects of the inhibition of $G\alpha_q$, phospholipase-C, and $G\beta\gamma$ on LPC(18:1)-induced Ca^{2+} signals (Supplementary Figure.5), suggesting LPC does not activate TRPV4 via G-protein-coupled receptor (GPCR) signaling.

We then conducted patch-clamp recordings of HEK293 cells overexpressing TRPV4 (rat, human), using the inside-out configuration, and demonstrated that LPC(18:1) activated TRPV4 at 54% of control currents evoked by TRPV4-selective agonist GSK101 (Figure.2*A-B*, Supplementary Figure.6*A*). We recorded a relevant underlying channel physiologic metric by conducting single-channel recordings in hTRPV4 expressing-HEK293 cells, namely that activation of TRPV4 by LPC(18:1) accounted for ~50% of the GSK101-evoked current (Figure.2*C*).

Based on previous observations that LPA interacts with the PIP_2-binding site of TRPV1[23], we also tested whether hTRPV4 with mutations in PIP_2-interaction sites affect activation by LPC(18:1). TRPV4 channels with mutations R269H[24] and 121AAWAA125[25] responded similarly as hTRPV4(WT) channels, demonstrating that these sites are not required for activation by LPC(18:1) (Figure. 2*D-G*).

TRPV1(K710) enables direct LPA-activation.[23] Alignment of TRPV1-TRPV4 (Figure.3*A*) identified rat/human-TRPV4(R746) and xenopus-TRPV4(R742) (TRPV4 structure xenopus-based[26]) as aligning with rTRPV1(K710), all within the highly conserved TRP-helix. We studied relevance of TRPV4(R746) for TRPV4-activation with affirmative results, using R746D charge-reversal, R746G inert-function mutation and a human arginine→cysteine polymorphism R746C (www.ncbi.nlm.nih.gov/clinvar/variation/VCV000450199.2) (Figure.3*B-D*, Supplementary Figure.6). All three R746-mutations activated normally with GSK101 (Supplementary Figure.6*C*, *E* and 7). Using biochemical assays, we also demonstrated LPC(18:1)-rTRPV4 binding, and observed a significant reduction of this interaction by R746D (Figure.3*E*). Taken together, these results strongly support that mammalian R746, located C-terminally in the TRP-helix, is required for TRPV4-activation by LPC.

We used this information to build a structure-based model of LPC(18:1)/xenopus-TRPV4 binding (Figure.3*F-G*, Supplementary Movie.1). Considering this structural prediction, we conducted glycine-mutagenesis of positively-charged residues K754, R757, R774 and W776 of rTRPV4, and recorded results suggesting relevance of each residue for TRPV4-activation by LPC(18:1) (Figure.3*H-I*). These results might indicate a direct interaction LPC(18:1)-TRPV4 as predicted. An alternative explanation is key relevance of these sites for activation of TRPV4 by LPC(18:1), yet binding elsewhere. Confirmation of our predicted binding site awaits future cryo-EM ultrastructural studies. Importantly, we found that the mutagenized sites did not affect GSK101 activating TRPV4 (Figure.3*H-I*), which likely functions via a different binding site (Supplementary Figure.8).

TRPV4-activation by LPC Induces ERK Phosphorylation, then Triggers Extracellular Release of miR-146a Through Rab5/Rab27a in Skin Keratinocytes

We next focused on downstream signaling of TRPV4-activation by LPC to determine the mechanism(s) by which activated keratinocytes relay the signal to skin-innervating pruriceptive afferents. We focused on MAP-kinase signaling based on our previous observations that MEK/ERK-activation can function downstream of TRPV4-mediated Ca^{2+}-influx in keratinocytes in response to pruritogens.[10] We detected rapidly increased ERK phosphorylation (pERK) in mouse and human keratinocytes 10min after LPC-stimulation (Figure.4*A-B*). This increase was TRPV4-dependent, based on effects of TRPV4-inhibitors on primary keratinocytes, and in-vivo in TRPV4 inhibitor-treated mice and keratinocyte-*Trpv4* cKOs (Figure.4*C*). Thus, TRPV4 is required for pERK increase-induced by LPC in keratinocytes. Pretreatment with MEK-inhibitor U0126 (i.d.) caused significant reduction in LPC-induced scratching (Figure.4*D*). Mice with a constitutively active B-raf transgene were used to address whether activation of MAP-kinases in skin keratinocytes suffices to elicit itch. Upon transgene induction, we observed significantly increased pMEK/pERK in skin and robust spontaneous scratching (Figure.4*E-G*). Thus, keratinocyte pERK is necessary and sufficient for LPC-induced itch.

We then queried paracrine-secretory functions of keratinocytes that underlie activation of skin-innervating pruriceptor nerve endings. We focused on secreted microRNAs (miRs) because miRs can signal paracrine directly via cell surface receptors such as toll-like receptors (TLRs) or TRP channels (e.g. TRPA1), which have been found expressed by peripheral sensory neurons and involved in itch and pain.[27, 28] We decided to test miR-let-7b, miR-125b-1, miR-16-5p, miR-203 and miR-146a because they are abundantly expressed in skin and involved in skin inflammation.[29, 30] We observed LPC evoked an increased release of miR146a from mouse and human keratinocytes (Figure.4*H-I*), but had no effect on other miRs (Supplementary Figure.9). In addition, miR-146a release was TRPV4- and MEK/ERK-dependent (Figure.4*H-I*). Our results agree with previous findings that MEK/ERK-inhibition suppresses vesicular biogenesis and secretion.[31] We then generated additional evidence for LPC-induced vesicular release and extracellular release of miR-146 by knocking-down Rab5a and Rab27a, both known components of the cellular vesicular release-machinery

and downstream targets of MEK/ERK in vesicular release,[31-33] which significantly attenuated both processes (Figure.4*J-L*)

miR-146a is a Pruritogen and Functions via TRPV1 in Primary Pruriceptor Neurons

To address whether miR-146a is pruritic, we i.d. injected mice and observed dose-dependent scratching (Figure.5*A*), not pain-related wiping (Figure.5*B*). This scratching response to miR-146a (4nmol/50µl) was immediate (latencies: 25sec (miR-146a) vs 55sec (LPC)), indicating non-delayed signaling of miR-146a to skin-innervating peripheral pruriceptor axons as opposed to an indirect mechanism such as gene regulation, as known for microRNAs. We next tested whether miR-146a-induced itch relied on $TRPV1^+$ pruriceptor-neurons, given the established role of TRPV1 in these neurons.[9] Selective ablation of $TRPV1^+$ central nerve terminals by i.t. injection of resiniferatoxin (Supplementary Figure.10) resulted in significantly reduced miR-146a-induced scratching, similar for LPC (Figure.5*C*). Thus the signaling chain LPC→keratinocyte-TRPV4→extracellularly-released miR-146a relies on $TRPV1^+$ pruriceptor neurons for causing itch. These results were extended by observing that miR-146a- or LPC-induced itch was significantly reduced by knockout or inhibition of TRPV1, but not TRPA1, indicating a reliance of pruritic effects of miR-146a and LPC on TRPV1 (Figure.5*D-G*). Notably, however, none of our TRPV1-targeting approaches completely eliminated scratching, suggesting additional contributory signaling mechanisms.

To elucidate sensory neuronal signaling in response to miR-146a, we recorded miR-146a-induced Ca^{2+}-influx in a dose-dependent manner in dissociated DRG neurons (Figure.6*A*). Ca^{2+}-influx depended on TRPV1 but not TRPA1, as observed when using selective inhibitors and *Trpv1*-KO and *Trpa1*-KO dissociated neurons (Figure.6*B*). We extended these findings to an organotypic DRG preparation, which enables Ca^{2+}-imaging via *Pirt*-promoter driven Ca^{2+}-indicator GCaMP3. miR-146a evoked a neuronal Ca^{2+}-transient in DRGs (Figure.6*C-E*, Supplementary Movie.2). Responsive neurons were ~12% of DRG neurons (Figure.6*G*), 72.7% of those were capsaicin-responsive (Figure.6*F*). % of miR-146a-responding neurons was significantly reduced when inhibiting TRPV1, not TRPA1 (Figure.6*G*).

These findings support the novel concept that extracellularly-released miR-146a from skin keratinocytes in response to LPC-induced TRPV4-activation activates skin-innervating TRPV1$^+$-pruriceptor neurons. Their peripheral epidermal projections are activated in a paracrine manner to elicit itch. Recent studies have demonstrated that extracellular miRs can either directly or indirectly via toll-like receptor 7 (TLR7) activate TRPA1 to elicit pain or itch[27, 28] and activation of TLR2/TLR6 heterodimers induces pain through TRPV1 and TRPA1.[34] Here, we could not corroborate that miR-146a-induced itch was significantly influenced by knockout or inhibition of TLR7 or inhibition of TLR2/6. In addition, we did not see significant Ca^{2+} influx upon stimulation with miR-146a in HEK293 cells transfected with rTRPV1 or co-transfected with rTRPV1 and rTLR7, 2, or 6 (Supplementary Figure.11).

Pruritic neural signaling can be attenuated by activation of kappa-opioid-receptors, which has gained in clinical relevance with anti-pruritic effects.[35] We recorded no effect of kappa-opioid-receptor agonism on LPC and miR-146a pruritogenicity, indicating their mutual independence (Supplementary Figure.12).

Future studies will elucidate mechanisms how miR-146a activates TRPV1$^+$-pruriceptor neurons at increased resolution.

LPC and miR-146a are Elevated in Cholestatic Pruritic Mice and in PBC Patients with Cholestatic Itch

Next we addressed the role of keratinocyte-TRPV4 in cholestatic itch and whether LPC and miR-146a function as pruritogens in a cholestasis disease-relevant context. We measured LPC and miR-146a levels in a mouse cholestasis model induced by systemic injection of α-naphthyl-isothiocyanate (ANIT).[5] We detected significantly increased LPC in both sera and skin (Figure.7*A*), and elevated systemic miR-146a in ANIT-treated mice (Figure.7*B*). ANIT-induced cholestatic itch (Figure.7*C*) was almost eliminated in keratinocyte-*Trpv4* cKOs. This indicates a key role for keratinocytes and keratinocyte-TRPV4 signaling in cholestatic itch. Moreover, systemic miR-146a was significantly reduced in keratinocyte-*Trpv4*-cKO ANIT-

mice (Figure.7*B*), indicating keratinocytes' release of miR-146a depended on cell-autonomous TRPV4-signaling.

We next measured LPC concentrations in sera of patients with PBC, an immune-mediated cholestatic liver disease with a high prevalence of pruritus, vs control patients with normal liver biopsies, observing no significant differences (Supplementary Figure.13). However, itch-phenotypic information was not available for these patients (Duke Health System).

We therefore tapped into patient biobank-repositories where itch-phenotypic information was readily available (Warsaw Medical University and University Hospital of Erlangen). We detected a significant increase of the vast majority of LPC species in sera of PBC patients with itch vs. no itch (Figure.7*D*). Itch intensity correlated with LPC concentrations ($R=0.4314$, $p<0.0029$, Figure.7*E*). We also found miR-146a levels were significantly elevated and correlated with itch intensity (Figure.7*F-G*). These findings, together with our other data, support the concept that upregulation of systemic LPC and miR-146a contributes to pruritus in PBC.

LPC and miR-146a evoke itch in nonhuman primates

We next addressed whether LPC and miR-146a are pruritogens in primates. Both molecules, upon i.d. injection, induced pruritus in rhesus monkeys in a dose-dependent manner (Figure.7*H*). This suggests that our new pruritus mechanism in mice and human primary keratinocytes extends to primates, further supporting our premise that LPC and miR-146a contribute to cholestatic itch.

Discussion

Here we describe a new signaling pathway of skin→sensory neuron-crosstalk relevant for cholestatic itch (Supplementary Figure.14). Our findings characterize the skin as a hitherto overlooked critical participant in cholestatic itch. Cholestatic itch has been viewed as the diseased liver generating pruritogenic mediators which then sensitize and activate pruriceptor sensory neurons to evoke perception of itch via neural

transmission.[3, 5, 8] Remarkably, this paradigm has not offered much as to (i) why the itch sensation originates from the epidermis, (ii) molecular mechanisms in skin cells, and (iii) how skin cells communicate with pruriceptor neurons' peripheral axons in cholestatic itch. Our findings provide an initial answer, and we deconstruct "forefront" signaling involving epidermal keratinocytes responding to LPC via TRPV4-activation, then signaling by extracellular release of miR-146a to $TRPV1^+$ skin-innervating peripheral nerve endings, activating these pruriceptors. We identified as novel pruritogen LPC, which is biosynthetically upstream of LPA, a previously-implicated pruritogen in cholestatic itch. Elevated LPC and miR-146a were detected systemically in PBC patients and mice with cholestatic itch. LPC and miR-146a were pruritic in mice and nonhuman primates. We observed that the pruritogenic effects of LPC and cholestatic itch in mice relied on keratinocyte-TRPV4. In addition, direct activation of TRPV4 by LPC led to Ca^{2+}-influx into keratinocytes which triggered MEK-ERK MAP-kinase signaling, which in turn evoked extracellular release of miR-146a relying on Rab5a and Rab27a, known components of the cellular vesicular release machinery.

Translational medical relevance rests on the following: Because LPC and miR-146a were elevated in the blood of PBC patients, the concept of LPC and miR-146a as possible biomarkers of cholestatic itch can now be addressed. Possibly our findings also apply to other hepatic pruritic diseases, another interesting subject for future studies. We note that elevated LPC was previously observed in patients with uremic pruritus[14], psoriasis[11, 12], and atopic dermatitis.[13] Back to cholestatic itch, this condition is almost certainly not mono-factorial. Most likely other metabolites function in a co-contributory manner, namely bilirubin, bile acids, LPA.[2, 3, 5, 6] However, it is clear that (i) LPC is a robust pruritogen, (ii) LPC has its own unique pathway in itch, yet conversion of LPC into LPA contributes to LPC pruritogenicity, (iii) systemic LPC concentrations are significantly elevated in pruritic PBC patients and correlated with itch intensity, and (iv) systemic and skin LPC concentrations are significantly elevated in cholestatic mice.

Furthermore pertinent to translation, several molecules in the readily-targetable integument can be targets, including TRPV4, TRPV1, MEK/ERK, and miR-146a. We also believe that our results of pruritogenicity of LPC and miR-146a in primates are relevant. Of note, a previous study in human volunteers demonstrated

that i.d. injection of LPC caused histopathology of skin irritation and inflammation, but pruritogenicity was not tested.[36] Decades before, LPC-evoked localized allergic inflammation in human skin was reported.[37]

Another recent study on TRPV4-expression in human chronic pruritus appears relevant. Chronic pruritus was associated with subjects' increased epidermal TRPV4-expression, and these patients had increased responses to capsaicin, including pruritus, burning/warmth sensation.[38] This finding, namely that increased TRPV4-expression in pruritic skin sensitizes TRPV1-signaling in sensory neurons, appears in agreement with our study.

Micro-RNAs are small, highly conserved, non-coding RNA molecules with known roles in RNA silencing and post-transcriptional regulation of gene expression.[39] Interestingly, recent work discovered an unconventional role for miRs: they can either directly or indirectly activate TRPA1 in sensory neurons to induce itch or pain.[27, 28] miR-146a has been found immunomodulatory in inflammation with postulated pro-resolution roles in psoriasis and atopic dermatitis, both of which are pruritic.[29, 30, 40] Our experiments support a new aspect of miR-146a in skin and sensory biology, namely that extracellular release of miR-146a from keratinocytes acts as 'transmitter' between keratinocytes and skin-innervating sensory neurons to primarily trigger itch. Indeed, i.d. injection of miR-146a elicited a more rapid scratching response (latency: ~25sec) than that of LPC (~55 sec), suggesting that (i) miR-146a induces itch without affecting gene regulation, and (ii) it functions downstream of LPC in itch. In addition, miR-146a did not elicit pain behavior in the mouse cheek model, indicating its selective activation of neural itch pathways. We reiterate that the mechanism how miR-146a activates $TRPV1^+$ sensory neurons needs to be further elucidated, especially miR-146a evoking itch, not pain.

Our findings are basic science-relevant. We implicated a putative new binding site for LPC(18:1) in the C-terminus of TRPV4, directly adjacent to the TRP-helix. The widely-used synthetic activator GSK101 does not bind here and activates heterologously-expressed TRPV4 with higher single channel conductance than the natural activator, LPC(18:1). Indeed, our discovery defines the first endogenous glycerophospholipid

activator of TRPV4. Given that GSK101 is lethal in-vivo[41], the quest for a therapeutically-beneficial (e.g. in arthritis, hepatic or renal disease) TRPV4 activator continues. Our discovery of a putative LPC(18:1)-TRPV4 binding site, awaiting confirmation in future structural studies, provides a framework for development of non-lethal TRPV4-activating molecules and inverse agonists. Also, TRPV4's gating mechanism can now be interrogated by comparing LPC(18:1) bound to TRPV4 vs GSK101 bound to TRPV4 using structural methods.

We view our discovery as a novel concept in the sensory submodality of cholestatic itch. The signaling mechanism we have unveiled is dependent on the following critical players: the innervated epithelia and the innervating pruriceptor sensory neuron, both of which rely on unexpected signaling molecules. We identified a hitherto non-recognized glycerophospholipid, LPC, as a pruritogen that initiates the signaling cascade in the skin, plus the messenger of the epithelia-sensory neuron crosstalk, an immunomodulatory micro-RNA, miR-146a, that directly activates pruriceptor sensory neurons. TRPV4 on keratinocytes and TRPV1 on pruriceptor sensory neurons function synergistically as key molecular players in this debilitating form of itch.

References

1. Dull MM, Kremer AE. Treatment of Pruritus Secondary to Liver Disease. Curr Gastroenterol Rep 2019;21:48.
2. Kremer AE, Martens JJ, Kulik W, et al. Lysophosphatidic acid is a potential mediator of cholestatic pruritus. Gastroenterology 2010;139:1008-18.
3. Lieu T, Jayaweera G, Zhao P, et al. The bile acid receptor TGR5 activates the TRPA1 channel to induce itch in mice. Gastroenterology 2014;147:1417-28.
4. **Abu-Hayyeh S**, **Ovadia C**, Lieu T, et al. Prognostic and mechanistic potential of progesterone sulfates in intrahepatic cholestasis of pregnancy and pruritus gravidarum. Hepatology 2016;63:1287-98.
5. Meixiong J, Vasavda C, Snyder SH, et al. MRGPRX4 is a G protein-coupled receptor activated by bile acids that may contribute to cholestatic pruritus. Proc Natl Acad Sci U S A 2019;116:10525-10530.
6. Yu H, Zhao T, Liu S, et al. MRGPRX4 is a bile acid receptor for human cholestatic itch. Elife 2019;8.
7. Noguchi K, Herr D, Mutoh T, et al. Lysophosphatidic acid (LPA) and its receptors. Curr Opin Pharmacol 2009;9:15-23.
8. Kittaka H, Uchida K, Fukuta N, et al. Lysophosphatidic acid-induced itch is mediated by signalling of LPA5 receptor, phospholipase D and TRPA1/TRPV1. J Physiol 2017;595:2681-2698.
9. Moore C, Gupta R, Jordt SE, et al. Regulation of Pain and Itch by TRP Channels. Neurosci Bull 2018;34:120-142.
10. Chen Y, Fang Q, Wang Z, et al. Transient Receptor Potential Vanilloid 4 Ion Channel Functions as a Pruriceptor in Epidermal Keratinocytes to Evoke Histaminergic Itch. J Biol Chem 2016;291:10252-62.
11. **Zeng C**, **Wen B**, **Hou G**, et al. Lipidomics profiling reveals the role of glycerophospholipid metabolism in psoriasis. Gigascience 2017;6:1-11.
12. Ryborg AK, Gron B, Kragballe K. Increased lysophosphatidylcholine content in lesional psoriatic skin. Br J Dermatol 1995;133:398-402.
13. Berdyshev E, Goleva E, Bronova I, et al. Lipid abnormalities in atopic skin are driven by type 2 cytokines. JCI Insight 2018;3:e98006.
14. Wu Q, Zhang H, Ding JR, et al. UPLC-QTOF MS-Based Serum Metabolomic Profiling Analysis Reveals the Molecular Perturbations Underlying Uremic Pruritus. Biomed. Res. Int. 2018;2018:4351674.
15. **Kim YS**, **Chu Y**, Han L, et al. Central terminal sensitization of TRPV1 by descending serotonergic facilitation modulates chronic pain. Neuron 2014;81:873-887.
16. Lee H, Ko MC. Distinct functions of opioid-related peptides and gastrin-releasing peptide in regulating itch and pain in the spinal cord of primates. Sci Rep 2015;5:11676.
17. Hamill OP, Marty A, Neher E, et al. Improved patch-clamp techniques for high-resolution current recording from cells and cell-free membrane patches. Pflugers Arch 1981;391:85-100.
18. Morales-Lázaro SL, Llorente I, Sierra-Ramírez F, et al. Inhibition of TRPV1 channels by a naturally occurring omega-9 fatty acid reduces pain and itch. Nat Commun 2016;7:13092.
19. Malik ZA, Liu TT, Knowlton AA. Cardiac Myocyte Exosome Isolation. Methods Mol Biol 2016;1448:237-48.
20. Kishimoto T, Soda Y, Matsuyama Y, et al. An enzymatic assay for lysophosphatidylcholine concentration in human serum and plasma. Clin Biochem 2002;35:411-6.
21. Kittaka H, Tominaga M. The molecular and cellular mechanisms of itch and the involvement of TRP channels in the peripheral sensory nervous system and skin. Allergol Int 2017;66:22-30.
22. **Moehring F**, **Mikesell AR**, Sadler KE, et al. Piezo1 Mediates Keratinocyte Mechanotransduction. bioRxiv 2020:2020.07.19.211086.
23. Nieto-Posadas A, Picazo-Juarez G, Llorente I, et al. Lysophosphatidic acid directly activates TRPV1 through a C-terminal binding site. Nat Chem Biol 2011;8:78-85.
24. Takahashi N, Hamada-Nakahara S, Itoh Y, et al. TRPV4 channel activity is modulated by direct interaction of the ankyrin domain to PI(4,5)P(2). Nat Commun 2014;5:4994.

25. **Garcia-Elias A**, **Mrkonjic S**, Pardo-Pastor C, et al. Phosphatidylinositol-4,5-biphosphate-dependent rearrangement of TRPV4 cytosolic tails enables channel activation by physiological stimuli. Proc Natl Acad Sci U S A 2013;110:9553-8.
26. Deng Z, Paknejad N, Maksaev G, et al. Cryo-EM and X-ray structures of TRPV4 reveal insight into ion permeation and gating mechanisms. Nat Struct Mol Biol 2018;25:252-260.
27. **Park CK**, **Xu ZZ**, **Berta T**, et al. Extracellular microRNAs activate nociceptor neurons to elicit pain via TLR7 and TRPA1. Neuron 2014;82:47-54.
28. **Han Q**, **Liu D**, Convertino M, et al. miRNA-711 Binds and Activates TRPA1 Extracellularly to Evoke Acute and Chronic Pruritus. Neuron 2018;99:449-463.e6.
29. Sonkoly E, Stahle M, Pivarcsi A. MicroRNAs: novel regulators in skin inflammation. Clin Exp Dermatol 2008;33:312-5.
30. Banerjee J, Sen CK. MicroRNAs in skin and wound healing. Methods Mol Biol 2013;936:343-56.
31. Datta A, Kim H, Lal M, et al. Manumycin A suppresses exosome biogenesis and secretion via targeted inhibition of Ras/Raf/ERK1/2 signaling and hnRNP H1 in castration-resistant prostate cancer cells. Cancer Lett 2017;408:73-81.
32. Colombo M, Raposo G, Théry C. Biogenesis, secretion, and intercellular interactions of exosomes and other extracellular vesicles. Annu Rev Cell Dev Biol 2014;30:255-89.
33. **Datta A**, **Kim H**, McGee L, et al. High-throughput screening identified selective inhibitors of exosome biogenesis and secretion: A drug repurposing strategy for advanced cancer. Sci Rep 2018;8:8161.
34. **Wang TT**, **Xu XY**, Lin W, et al. Activation of Different Heterodimers of TLR2 Distinctly Mediates Pain and Itch. Neuroscience 2020;429:245-255.
35. Tseng PY, Hoon MA. Molecular Genetics of Kappa Opioids in Pain and Itch Sensations. Handb Exp Pharmacol 2020.
36. Ryborg AK, Deleuran B, Sogaard H, et al. Intracutaneous injection of lysophosphatidylcholine induces skin inflammation and accumulation of leukocytes. Acta Derm Venereol 2000;80:242-6.
37. Middleton E, Jr., Phillips GB. Release of histamine activity in human skin by lysolecithin. J Lab Clin Med 1964;64:889-94.
38. **Hidding J**, **Agelopoulos K**, Pereira MP, et al. Sensory Qualities Point to Different Structural and Functional Skin Patterns in Chronic Pruritus Patients. A Translational Explorative Study. Acta Derm Venereol 2019;99:668-674.
39. Bartel DP. MicroRNAs: genomics, biogenesis, mechanism, and function. Cell 2004;116:281-97.
40. Rebane A, Runnel T, Aab A, et al. MicroRNA-146a alleviates chronic skin inflammation in atopic dermatitis through suppression of innate immune responses in keratinocytes. J Allergy Clin Immunol 2014;134:836-847.e11.
41. Pankey EA, Zsombok A, Lasker GF, et al. Analysis of responses to the TRPV4 agonist GSK1016790A in the pulmonary vascular bed of the intact-chest rat. Am J Physiol Heart Circ Physiol 2014;306:H33-40.

(Author names in bold designate shared co-first authorship)

Figure 1. LPC-, but not LPA-, induced scratching behavior requires *Trpv4* in skin keratinocytes.

(*A*) LPA(18:1)-induced itch was not significantly altered in mice: *Trpv4*-KO, wildtype (WT) i.p. pretreated with TRPV4-inhibitors GSK205 (20mg/kg) or HC067047 (20mg/kg), sensory neuron-*Trpv4*-cKO (Nav1.8-Cre::Trpv4$^{fl/fl}$), or keratinocyte-*Trpv4*-cKO (K14-Cre::Trpv4$^{fl/fl}$, tamoxifen (tam)-inducible). n=4-7 mice/ group.

(*B*) LPC(egg-LPC) elicited dose-dependent scratching. **p<0.01 and ***p<0.001 vs. normal saline (NS), n=5 mice for NS and 50µg, 6 for 150µg, and 11 for 500µg.

(*C*) Note LPC induced robust scratching (itch), not wiping (pain) response in the mouse cheek model. ***p<0.001 vs. NS, n=4-5 mice/group.

(*D*) LPC induced itch that was not significantly attenuated in *Trpv4*-KOs or in sensory neuron-*Trpv4*-cKOs, but significantly reduced in WTs i.p. pretreated with GSK205 (20mg/kg) or HC067 (20mg/kg) and in keratinocyte-*Trpv4*-cKOs. *p<0.05 and **p<0.01 vs. WT LPC, n=7-11 mice/group.

(*E*) Different species of LPC also evoked robust scratching, with LPC(18:1) most potent (n=5 mice/ species except n=11 for LPC).

(*F*) LPC(18:1)-evoked scratching was also significantly reduced in keratinocyte-*Trpv4*-cKOs. ***p<0.001 vs. WT, n=4-5 mice/group.

(*G*) I.t. injection of LPC did not elicit scratching, n=5 mice/group.

(*H*) LPC-induced itch was attenuated in WTs by i.p.-pretreatment with autotaxin-inhibitor PF8380 (10mg/kg), and this attenuation was further augmented in keratinocyte-*Trpv4*-cKOs. **p<0.01 and $^{\#}$p<0.05, n=8-11 mice/group.

(*I-L*) LPC-induced Ca^{2+}-influx in a dose-dependent manner in mouse (I) and human (K) keratinocytes (KC). LPC-induced Ca^{2+}-influx was significantly reduced by GSK205 or HC067047 (10µM, J, L) and in KC from keratinocyte-*Trpv4*-cKO (J). *p<0.05, **p<0.01 and ***p<0.001 vs. LPC, n≥180 cells recorded/treatment.

(*M-P*) LPA(18:1)-induced Ca^{2+}-influx was not dose-dependent and was less robust than that of LPC in mouse (M) and human (O) KC. In addition, LPA(10µM)-induced Ca^{2+}-signal remained unchanged with GSK205 or HC067047 pretreatment (10µM, N, P) or in KC from keratinocyte-*Trpv4*-cKO (N). n≥200 cells recorded/treatment.

Two-tailed t-test for C and one-way ANOVA with Tukey's post-hoc-test for the rest.

Figure 2. LPC directly activates TRPV4 channels.

(*A-B*) Representative current-time plots from excised inside-out membrane-patches in rTRPV4-transfected HEK cells. These were obtained initially without agonist (gray), in the presence of LPC(18:1) (blue) or TRPV4 agonist GSK1016790A (GSK101; black). (A) Traces shown were recorded at -60 and +60mV. (B) Current-voltage relationships from -120 to +120mV. N=5 cells/condition.

(*C*) Single-channel recordings (left) of hTRPV4 activated with GSK101 or LPC(18:1) at +60mV, o=open, c=closed state of TRPV4; all-point histograms obtained from the traces (right). The average for the open level amplitudes was 6.45±0.55pA with an open probability of 0.85±0.08 for GSK101, and 3.27±0.41pA and 0.75±0.08 for LPC(18:1). N=5 cells/condition.

(*D-G*) Activation of hTRPV4 by LPC(18:1) remained unchanged with PIP2-interaction-mutations. (D-F) Representative currents for hTRPV4(WT), hTRPV4(R269H), and hTRPV4(121AAWAA125) channels. Currents were obtained initially without agonist (grey), in the presence of LPC(18:1) (blue, sky blue and orange, respectively) or GSK101 (black) at -60 and +60mV. (G) There were no significant differences in currents among hTRPV4(WT), hTRPV4(R269H), and hTRPV4(121AAWAA125) in response to LPC(18:1); data normalized to activation with GSK101. N=5-6 cells/condition; one-way ANOVA with Tukey's post-hoc-test for (G).

Figure 3. LPC activates TRPV4 directly via a C-terminal binding pocket.

(*A*) Sequence alignment of the C-terminus comprising the TRP helix of rTRPV1, xenTRPV4, rTRPV4 and hTRPV4. Note conservation of positive charge at position K710 for TRPV1, R742 for xenTRPV4, and R746 for rTRPV4 and hTRPV4 (in red). Identical residues, shared between TRPV1 and TRPV4, C-terminal of this key residue are bolded in black. Identical residues, conserved only in vertebrate TRPV4, C-terminal to R742/R746 are bolded in purple.

(*B-E*) Representative currents from excised inside-out membrane-patches in rTRPV4-transfected HEK cells (B) or rTRPV4(R746D) (C) were obtained without agonist stimulation (gray), in the presence of LPC(18:1) (blue, red) or TRPV4 agonist GSK1016790A (GSK101, black). Traces shown were obtained at -60 and +60

mV. (D) There was a significant current reduction in rTRPV4(R746D)-transfected HEK cells when activated with LPC(18:1). Data were normalized to activation with GSK101. ***p<0.001 vs. rTRPV4, n=5 cells/group. (E) In-vitro interaction assays show significantly reduced binding of LPC(18:1) to rTRPV4(R746D) . ***p<0.001 vs. rTRPV4, n=3 assays/group.

(*F-G*) Based on alignment and established TRPV4-structure (crystal, cryo-EM), derived from Xenopus tropicalis TRPV4, note our structural model that explains binding of LPC(18:1) to a series of positively charged AA750-772; with R742 as a postulated structural determinant of this binding. Left-hand rendering shows the TRPV4-tetramer (each subunit in different color) as it integrates into the plasma membrane, with the green subunit binding of LPC(18:1). Right-hand schematic shows binding of LPC(18:1) to the TRPV4 C-terminus at higher resolution.

(*H-I*) The Ca^{2+}-signal induced by LPC(18:1) was drastically reduced in TRPV4-transfected HEK cells (TRPV4-mutations R746C, R746G, R746D, K754G, R757G, R774G, W776G). In contrast, GSK101-induced Ca^{2+}-signal was not significantly disrupted, except a moderate reduction with mutation W776G. **p<0.01 and ***p<0.001 vs. EGFP, $^{\#}$p<0.05 and $^{\#\#}$p<0.01 vs. hTRPV4 or rTRPV4, n≥120 cells recorded/condition.

Two-tailed t-test for D-E, one-way ANOVA with Tukey's post-hoc-test for H-I.

Figure 4. LPC elicits extracellular release of miR-146a from skin keratinocytes depending on TRPV4→pERK→Rab5a/Rab27a signaling.

(*A-B*) Note LPC-induced increase of pERK in cultured mouse keratinocytes (KC, (A)) and human KC (B) and its elimination by pretreatment with TRPV4 inhibitors GSK205 and HC067047 (10µM). *p<0.05 vs veh. (0.2% DMSO). $^{\#}$p<0.05 and $^{\#\#}$p<0.01 vs. LPC, n=4-6 cultures/group (5-7 pups/culture for mice, 2 subjects/culture for human).

(*C*) I.d. LPC-injection (500µg/50µl) increased pERK in dissected dorsal neck skin that was reversed by i.p. pretreatment with GSK205 (20mg/kg) and in keratinocyte-*Trpv4*-cKOs. *p<0.05 vs Veh. (normal saline), $^{\#\#}$p<0.01 vs. LPC, n=7 mice/group.

(*D*) LPC-induced scratching was significantly attenuated by i.d.-pretreatment with MEK-selective inhibitor U0126 (20µg/50µl). ***p<0.001 vs LPC, n=11 mice for LPC, n=6 for U0126+LPC.

(*E*) Note increased p-MEK expression in dorsal neck skin 2d after induction of the B-raf transgene by 4-OH-tamoxifen treatment (arrows: epidermis; blue: DAPI).

(*F*) Western-blot revealed increased p-ERK in dorsal neck skin 2d after induction of the B-raf transgene. **p<0.01 vs. veh., n=4 mice for veh. and n=7 for tamoxifen.

(*G*) Induction of B-raf transgene in skin KC elicited robust scratching on d2. *p<0.05 vs. veh., n=5 mice for veh. and n=8 for tamoxifen.

(*H*) LPC-induced extracellular release of miR-146a from cultured mouse and human KC was eliminated by pretreatment with GSK205 or HC067047 (10µM). *p<0.05 vs. veh., $^{\#}$p<0.05 and $^{\#\#}$p<0.01 vs. LPC, n=3-4 cultures/treatment (5-7 pups/culture for mice, 2 subjects/culture for human).

(*I*) LPC-induced extracellular release of miR-146a from cultured mouse and human KC was eliminated by pretreatment with U0126 (10µM). *p<0.05 vs. veh., $^{\#}$p<0.05 and $^{\#\#}$p<0.01 vs. LPC, n=3-4 cultures/treatment (5-7 pups/culture for mice, 2 subjects/culture for human).

(*J*) LPC-induced extracellular vesicular release from cultured mouse KC was eliminated by U0126 (10µM). **p<0.01 vs. control, $^{\#\#}$p<0.01 U0126+LPC vs. LPC; n=4-6 cultures (5-7 pups/culture).

(*K*) Experimental setup as in (J), we detected a significant decrease of LPC-induced vesicular release from mouse KC treated with Rab27a- or Rab5a-siRNA (scrambled-siRNA control set '1' for relative comparison). *p<0.05 vs scramble+LPC. N=4-6 cultures (5-7 pups/culture).

(*L*) RT-qPCR assay detected a significant decrease of LPC-induced release of miR-146a from mouse KC by siRNA-mediated knockdown of Rab27a or Rab5a. *p<0.05 vs scramble+LPC. n=4-5 cultures (5-7 pups/culture).

One-way ANOVA with Tukey's posthoc-test was used for A-C, G, H-L, two-tailed t-test for D, F.

Figure 5. miR-146a elicits scratching behavior, which requires TRPV1, but not TRPA1, in sensory neurons.

(*A*) miR-146a induced dose-dependent scratching behavior, but scramble-control did not cause significant scratching behavior. *p<0.05 and ***p<0.001 vs. normal saline (NS), n=4-5 mice/group.

(*B*) The mouse cheek model demonstrated that miR-146a elicited robust scratching (itch) but not wiping response (pain). ***p<0.001 vs. NS, n=4-5 mice/group.

(*C*) Elimination of TRPV1-expressing spinal nerve terminals using i.t. injection of resiniferatoxin (RTX, 200ng/5µl) significantly reduced miR-146a- or LPC-induced itch. *p<0.05 and **p<0.01 vs. veh. (2%EtOH+2%Tween-80), n=4-5 mice/group except n=11 for veh.+LPC .

(*D-E*) miR-146a- and LPC-induced itch were significantly attenuated by i.p. (2mg/kg) or i.t. (30µg) injection of the TRPV1-inhibitor SB366791, or in *Trpv1*-KO. *p<0.05 and **p<0.01 vs. WT, n=4-5 mice/group for (D) and n=6-11 mice/group for (E).

(*F-G*) miR-146a- and LPC-induced itch were not significantly altered by i.p. (30mg/kg) or i.t. (30µg) injection of the TRPA1-inhibitor HC030031, or in *Trpa1*-KO. n=4-5 mice/group for (F) and n=5-11 mice/group for (G). One-way ANOVA with Tukey's post-hoc-test was used for A, D-G, two-tailed t-test for B-C.

Figure 6. miR-146a activates primary sensory neurons in a TRPV1-, but not TRPA1-, dependent manner.

(*A*) miR-146a induced Ca^{2+}-influx in cultured DRG neurons in a dose-dependent manner (arrow: miR-146a or scramble stimulation). n≥190 neurons recorded/concentration.

(*B*) miR-146a (300nM) induced Ca^{2+}-influx that was significantly reduced by pretreatment with TRPV1-inhibitor SB366791 (10µM) and in neurons from *Trpv1*-KOs, but not significantly altered by TRPA1-inhibitor HC030031 (10µM) or in neurons from *Trpa1*-KOs. **p<0.01 vs. scramble (300nM) and $^{\#}$p<0.05 vs. miR-146a, n≥190 neurons recorded/concentration.

(*C*) Representative Ca^{2+}-imaging of GCaMP3-expressing DRG neurons in an ex-vivo preparation illustrates the increased Ca^{2+}-signal following stimulation with miR-146a (300nM) and capsaicin (1µM).

(*D*) Representative Ca^{2+}-traces of miR-146a(+)/capsaicin(-), miR-146a(+)/capsaicin(+), or miR-146a(-)/capsaicin(+) DRG neurons.

(*E*) Representative Ca^{2+}-traces of a population of DRG neurons responsive to miR-146a.

(*F*) Of 1250 neurons recorded, 154 were responsive to miR-146a. 72.7% of miR-146a-responsive neurons were also capsaicin-responsive.

(*G*) Increased percentage of total DRG neurons responding to miR-146a (300nM) was significantly reduced by SB366791 (10μM), but not by HC030031 (10μM). **p<0.01 vs. scramble-control (300nM) and $^{\#}$p<0.05 vs. miR-146a, n=4-9 DRG explants/group (1 explant /mouse).

One-way ANOVA with Tukey's post-hoc-test was used for B, G.

Figure 7. LPC and miR-146a are elevated in mice or primary biliary cholangitis (PBC) patients with cholestatic itch and induce itch in nonhuman primates.

(*A*) ANIT-treatment increased LPC levels in both serum and skin. **p<0.01 and ***p<0.001 vs. WT-control, two-tailed t test, n=5-8 mice/group.

(*B*) ANIT-treatment increased miR-146a in serum, which was attenuated in keratinocyte-*Trpv4*-cKOs. *p<0.05 vs. WT-control, and $^{\#}$p<0.05 vs keratinocyte-*Trpv4*-cKOs, one-way ANOVA with Tukey's post-hoc-test. N=8-11 mice/group.

(*C*) ANIT-induced cholestatic itch was significantly attenuated in keratinocyte-*Trpv4*-cKOs, *p<0.05, **p<0.01, ***p<0.001 vs. WT-control, $^{\#}$p<0.05 vs. $^{\#}$p<0.05 vs keratinocyte-*Trpv4*-cKOs, two-way ANOVA with Tukey's post-hoc-test. N=6 mice/group.

(D) All detected LPC species, except for LPC(20:4), were significantly elevated in PBC patients' sera with itch (n=27) vs. without itch (n=21), *p<0.05 and **p<0.01, two-tailed t-test.

(*E*) When all detected LPC species from individual patients were aggregated, there was a significant correlation of total LPC concentration with the itch intensity. Pearson's correlation coefficient: R= 0.4314, p=0.0029.

(*F*) A significant increase in abundance of miR-146a was detected in sera of PBC patients with itch (n=10) vs. without itch (n=12), **p<0.01, two-tailed t-test.

(*G*) Note a significant correlation of miR-146a level with the itch intensity. Pearson's correlation coefficient: R= 0.4536, p=0.034.

(*H*) LPC or miR-146a induced scratching behavior in rhesus monkeys in a dose-dependent manner. Histamine was used as positive control. ***p<0.001, $^{\#}$p<0.05, $^{\#\#}$p<0.01, and $^{\$\$\$}$p<0.001 vs. normal saline (NS), repeated measures using a linear-mixed-model; n=9 monkeys/group.

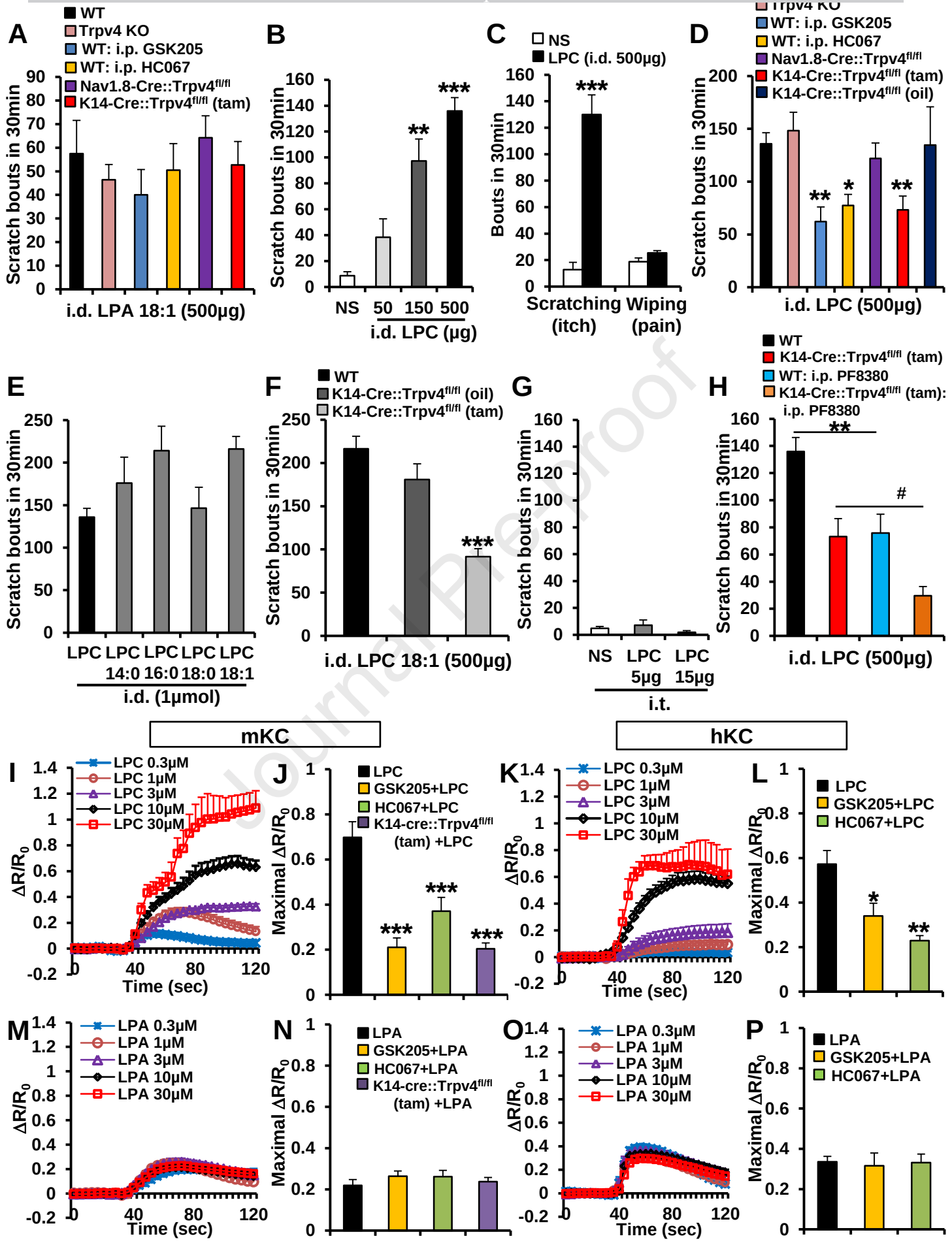

Figure 1

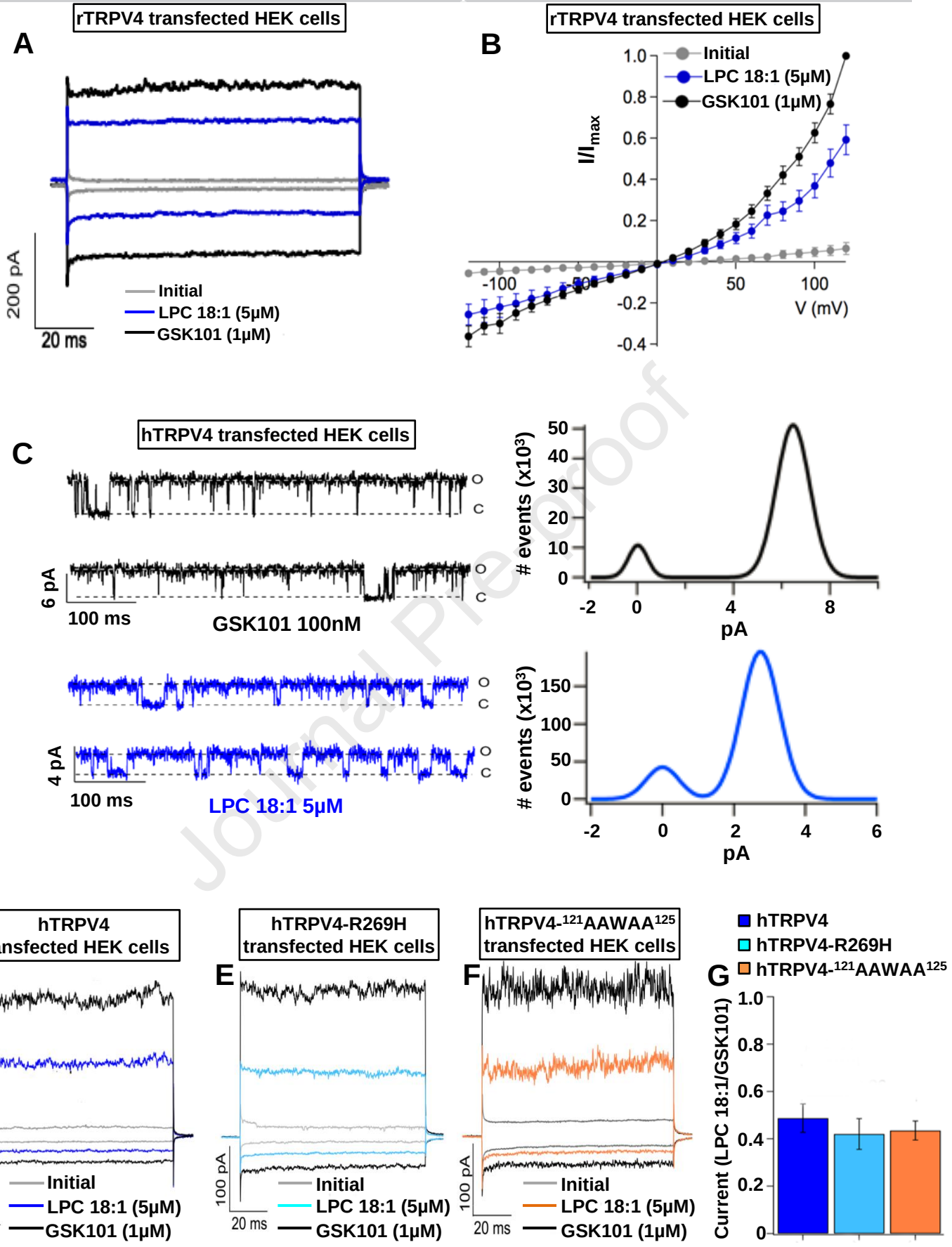

Figure 2

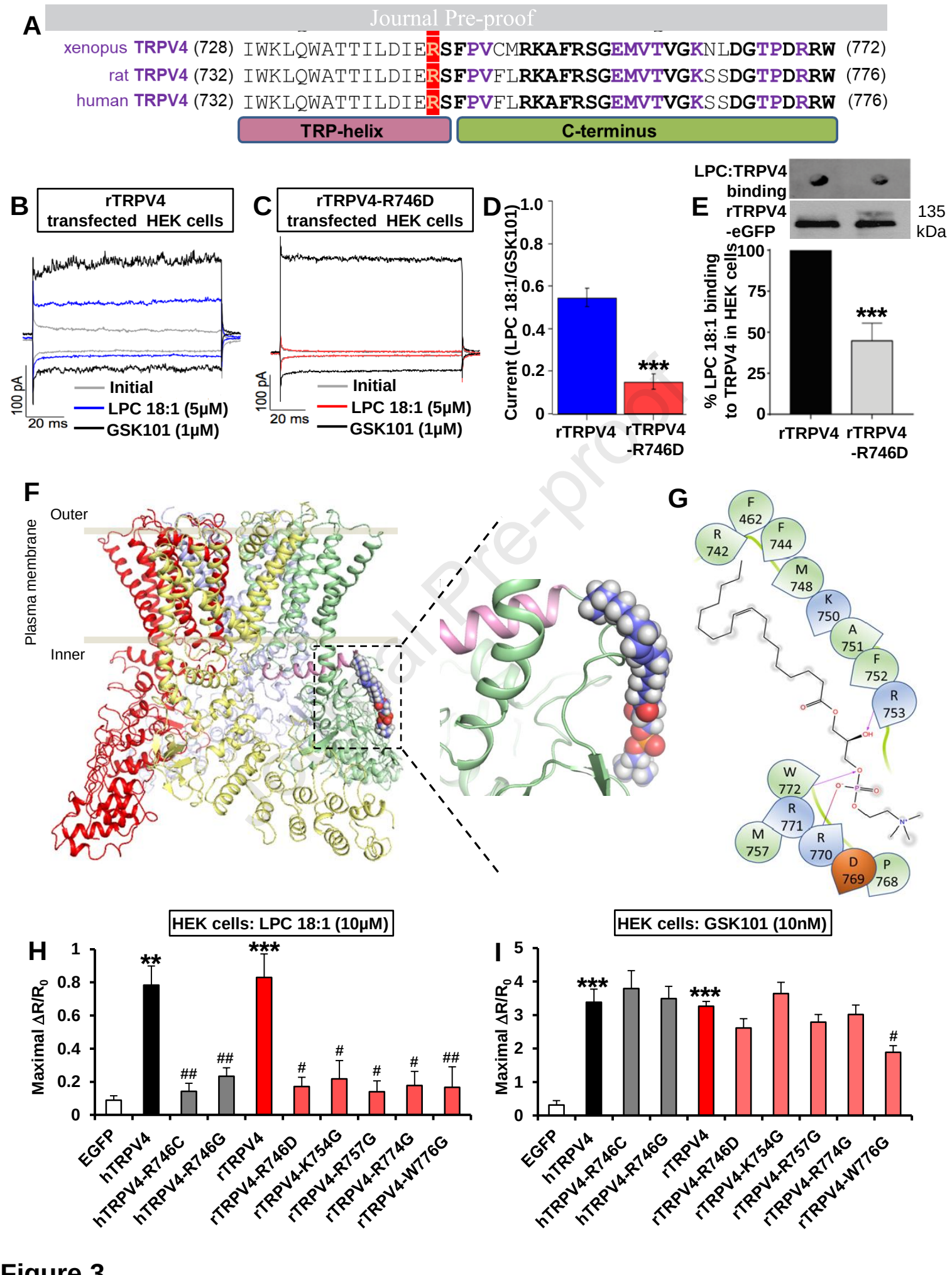

Figure 3

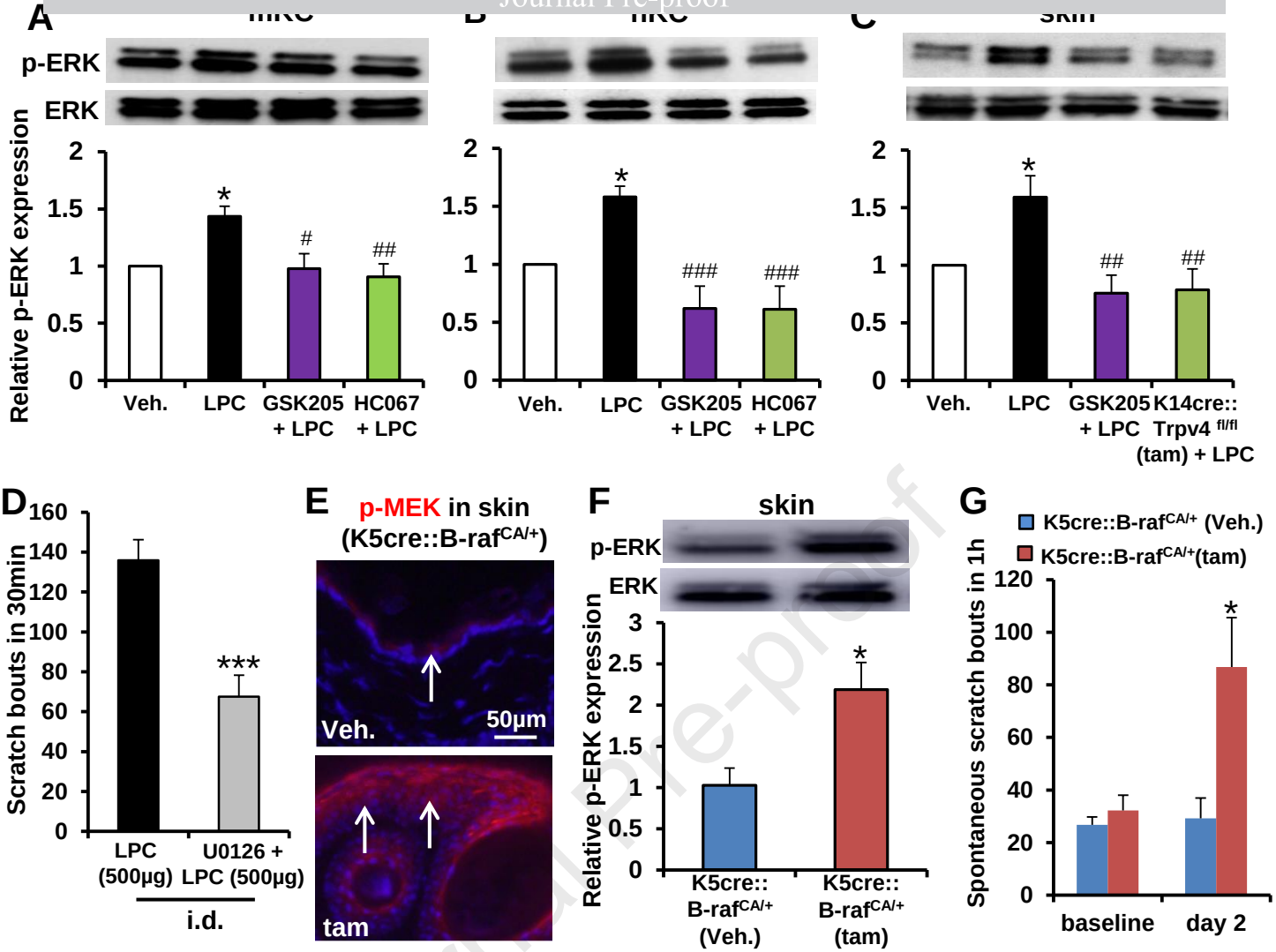

Figure 4

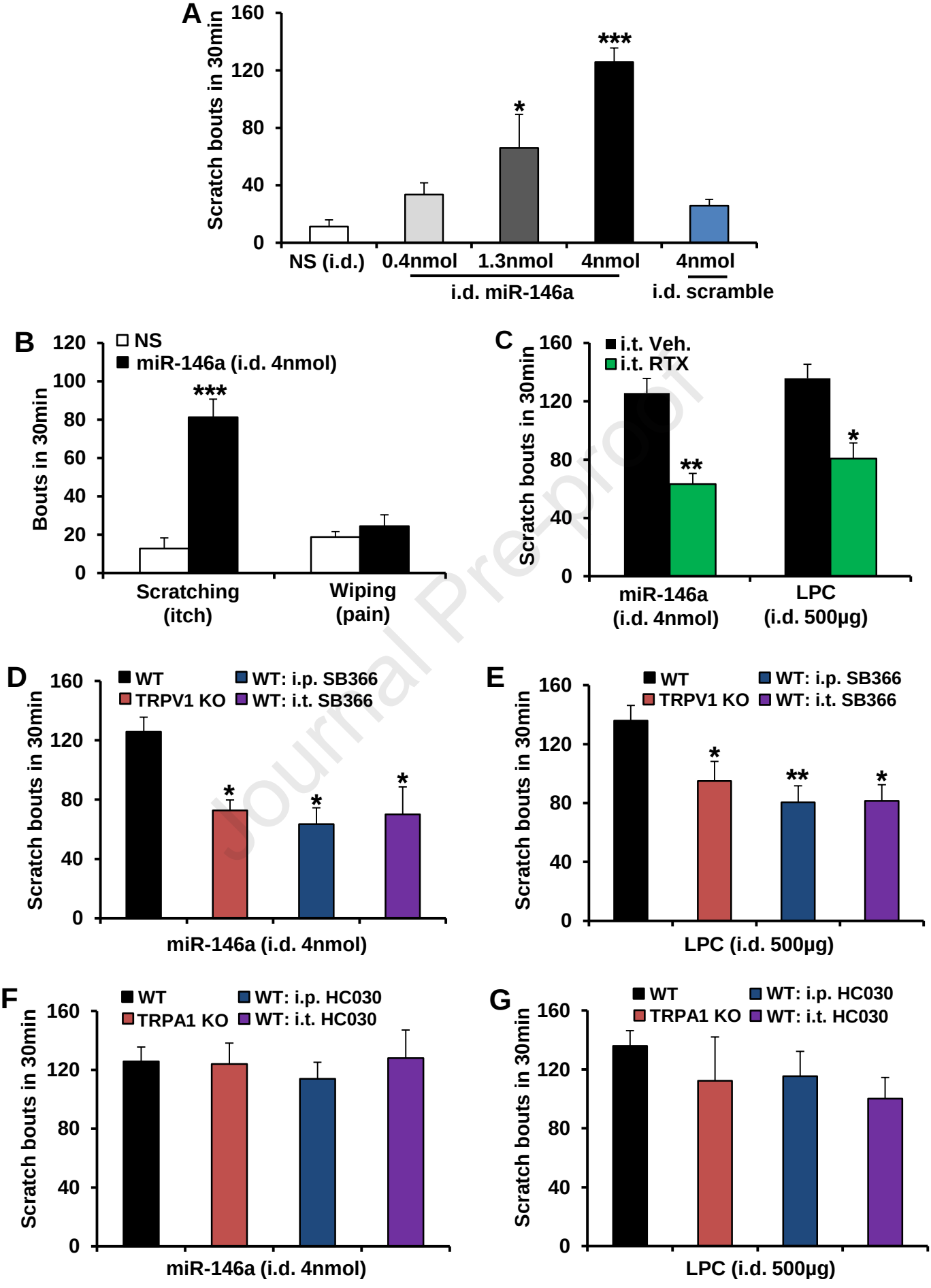

Figure 5

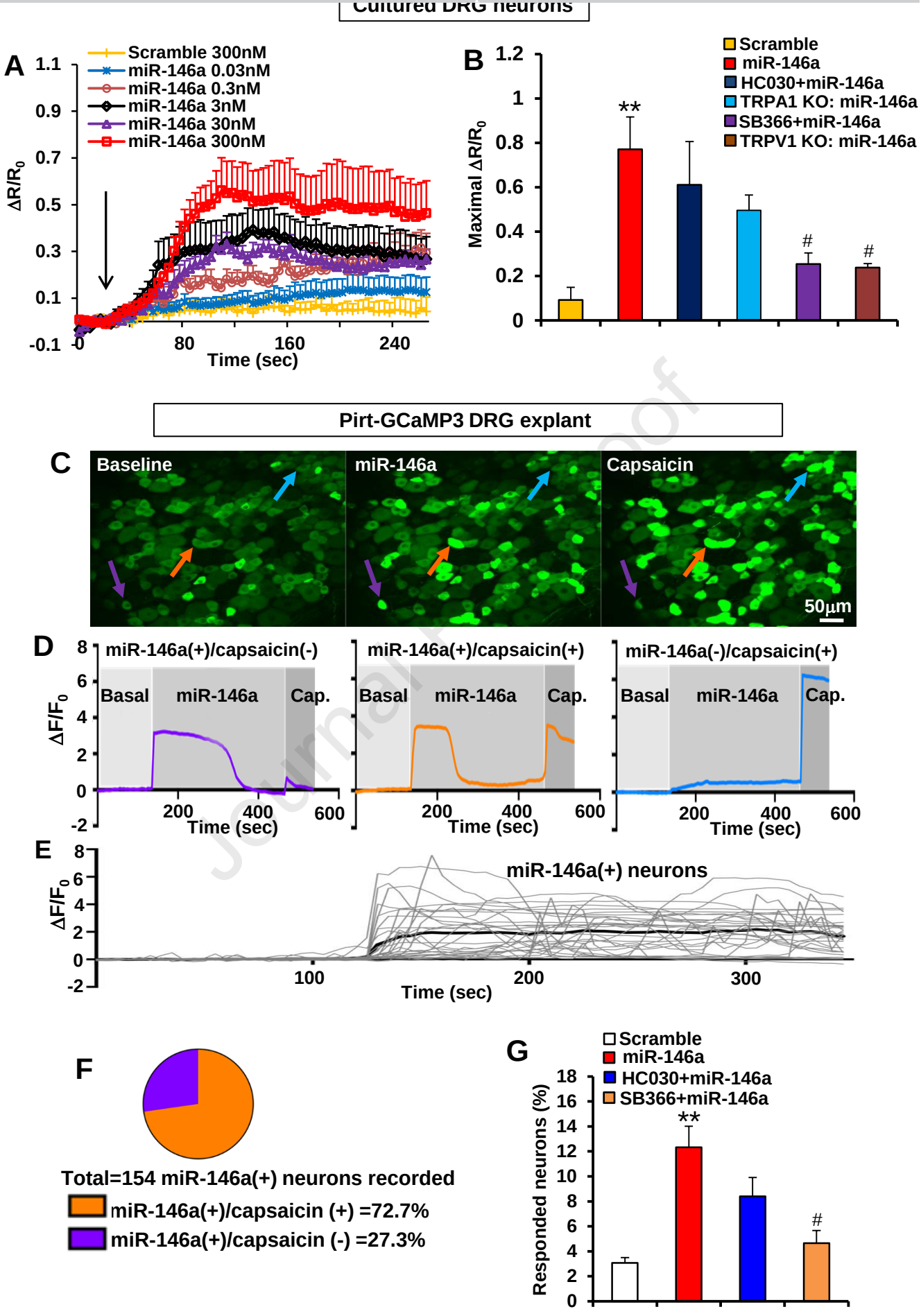

Figure 6

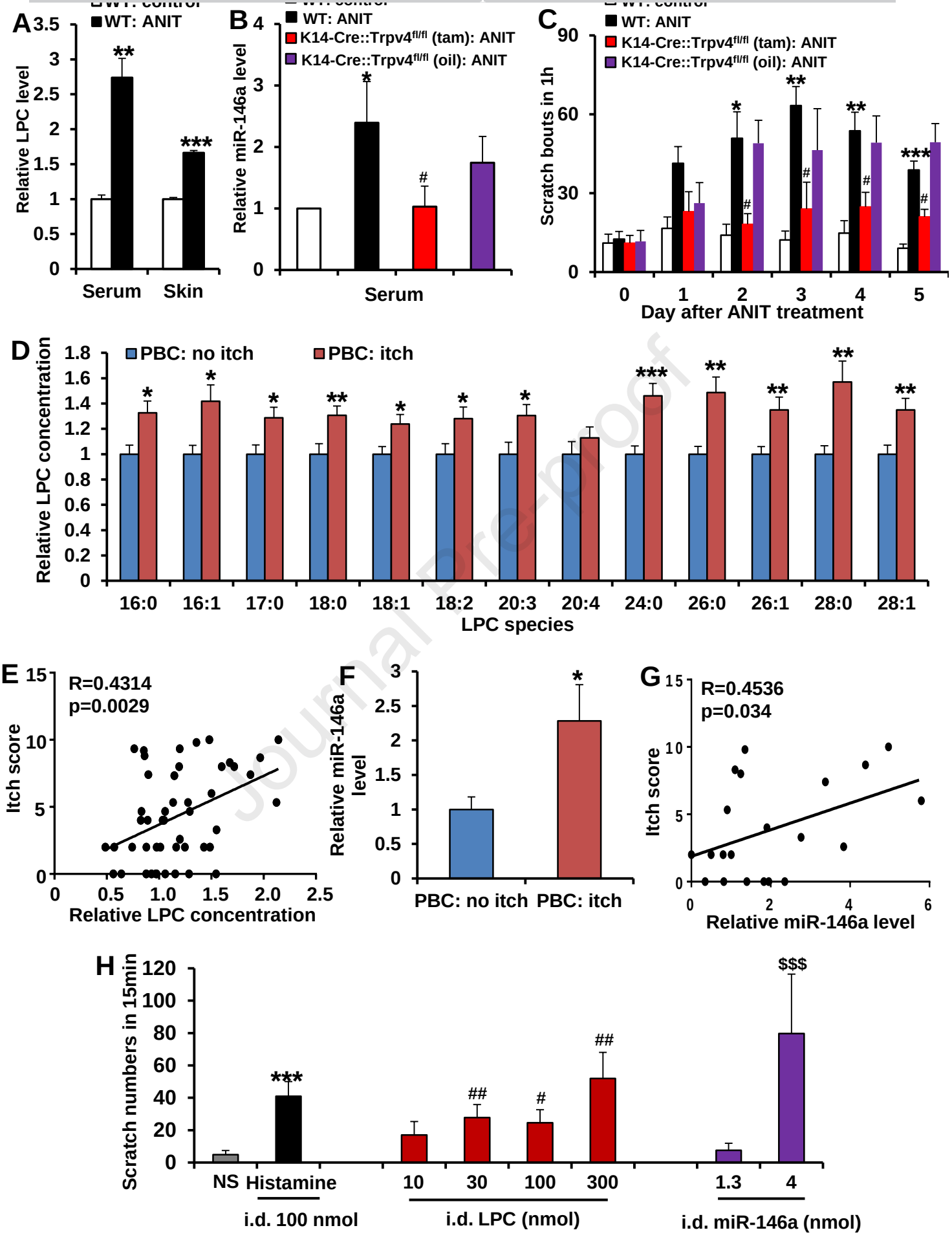

Figure 7

ms. GASTRO-D-20-03666

In case of acceptance we have prepared the following:

— what you need to know summary

BACKGROUND AND CONTEXT
Mechanistic understanding of cholestatic pruritus is lacking, for example in primary biliary cholangitis (PBC), an autoimmune hepatopathy.

NEW FINDINGS
Lysophosphatidylcholine (LPC) functioned as a novel cholestatic pruritogen. As mechanism, LPC directly activates TRPV4 ion channels of skin keratinocytes, which triggers the release of miR-146a to activate $TRPV1^+$ pruriceptor neurons.

LIMITATIONS
How miR-146a activates $TRPV1^+$ pruriceptor neuron needs to be further elucidated.

IMPACT
LPC functions as pruritogen with potential impact in PBC. Our new LPC→TRPV4-based mechanism supports the novel concept of the skin as a forefront sensory organ, relevant in cholestatic itch.

— Lay summary

We identified lysophosphatidylcholine as a novel itch-causing endogenous phospholipid with potential key impact on itch of chronic liver disease. We also uncovered lysophosphatidylcholine's cognate receptor in skin, calcium-permeable TRPV4 channels.

Supplementary Materials and Methods

Animals

Wild-type (WT) C57bl/6j mice were purchased from the Jackson Laboratory. *Trpv4* knockout (KO) mice were generated in our laboratory as previously described.[1] *Trpv1* KO (Stock No: 003770), *Trpa1* KO (Stock No: 006401), and *Tlr7* KO (Stock No: 008380) mice, originally obtained from the Jackson Laboratory, were provided by Dr. Ru-Rong Ji at Duke University. Pirt-GCaMP3 mice,[2] originally generated by Dr. Xinzhong Dong at Johns Hopkins University, were provided by Dr. Andrea Nackley at Duke University. Pirt-GCaMP3 mice express the calcium indicator, GCaMP3, in >96% of primary sensory neurons in the dorsal root ganglion (DRG) and trigeminal ganglion (TG).

Keratinocyte-specific, tamoxifen (tam)-inducible *Trpv4* knockout mice were used as previously described.[3-5] In brief, the *Trpv4* genomic locus was engineered so that loxP sites surrounded exon 13, which encodes TM5–6. This mutation was propagated in mice that were crossed to K14-Cre-ER^{tam} mice, so that K14-Cre-ER^{tam}::*Trpv4*$^{lox/lox}$ mice could be induced by tamoxifen (tam) administration via oral gavage for five consecutive days at 5 mg/day in 0.25 ml corn oil at 2–2.5 months of age, plus a booster 2 weeks after the last application. Control animals received the same volume of corn oil. Efficiency of targeting was verified by quantitative real-time PCR and immunohistochemistry for *Trpv4* expression in skin at gene and protein levels, respectively.[3]

We also generated mice with deletion for *Trpv4* in primary sensory neurons via Cre-loxP-mediated recombination by mating mice carrying *Trpv4* (*Trpv4*$^{fl/fl}$) with a mouse line expressing Cre recombinase under control of the *Nav1.8* promoter (*Nav1.8-Cre*). The *Cre* mice enable gene recombination commencing at birth selectively in sensory neurons expressing the sodium channel Nav1.8, without affecting gene expression in the spinal cord, brain, or any other organ in the body.[6] Efficiency of targeting was verified by quantitative real-time PCR and

immunohistochemistry for *Trpv4* expression in both DRGs and TGs at gene and protein levels, respectively (Supplementary Figure.1).

We also generated mice with inducible expression of constitutively active B-raf(V600E) in keratinocytes by crossing mice with a floxed allele for B-raf (B-raf$^{CA/+}$ mice) [7] with K5-cre-ER^{tam} mice.[8] The generated K5-cre-ER^{tam}::Braf$^{CA/+}$ mice (provided by Dr. Jennifer Zhang at Duke Uni.) were shaved at the dorsal back and topically treated with 4-hydroxy tamoxifen (100 µl of 20 mg/ml) in ethanol (EtOH) for 2 consecutive days. Control animals received the same volume of EtOH. Increased levels of p-MEK and p-ERK, downstream targets of B-raf, were detected in skin after treatment with 4-hydroxy tamoxifen, as verified by immunohistochemistry or Western blot (Figure. 4E-F).

Mice were housed in climate-controlled rooms on a 12/12-h light/dark cycle with water and a standardized rodent diet available *ad libitum*. All animal protocols were approved by the Duke University Institutional Animal Care and Use Committee (IACUC) in compliance with National Institutes of Health (NIH) guidelines. All of these mouse lines have C57bl/6 background and were PCR-genotyped before use. Only male mice (2-3 months old) were used for *in vivo* behavioral assays.

In addition, adult male and female rhesus monkeys (*Macaca mulatta*, 11-18 years, 7.2-13.9 kg), were used for scratching behavior study. Monkeys were individually housed in species-specific and climate-controlled rooms on a 12/12-h light/dark cycle. Their daily diet consisted of approximately 22-30 biscuits (Purina Monkey Chow; Ralston Purina Co., St. Louis, MO), fresh fruit, and water *ad libitum*. Monkeys were kept at an indoor facility accredited by the Association for Assessment and Accreditation of Laboratory Animal Care International (Frederick, MD, USA). All animal care and experimental procedures were conducted in accordance with the Guide for the Care and Use of Laboratory Animals as adopted and promulgated by NIH and approved by

the IACUC of Wake Forest University. This study is reported in accordance with the ARRIVE guidelines for reporting experiments involving animals.

Human subjects

No-liver-disease controls and primary biliary cholangitis (PBC) patients with unknown itch status were recruited via the Duke Gastroenterology-Hepatology outpatient program, non-alcoholic fatty liver disease (NAFLD) clinical research program. Controls had normal liver histology, and PBC patients were diagnosed according to the European Association for the Study of Liver Disease criteria.[9] The study population consisted of 27 women and 8 men, aged 24-65 years (average 44) for controls and 25 women and 0 men, aged 39-83 years (average 58) for PBC.

Primary biliary cholangitis (PBC) patients with known itch-phenotypic information were recruited at two clinical sites: Liver and Internal Medicine Unit of the Warsaw Medical University, Poland, and Department of Medicine 1, Gastroenterology, Hepatology, Pneumology and Endocrinology of the University Hospital of Erlangen, Germany. The diagnosis of PBC was made according to the European Association for the Study of Liver Disease criteria.[9] Itch intensity was quantified at the time-point of blood drawing using a visual analogue scale ranging from 0 to 10 (0-3: no/mild itch, 3-6: moderate itch, 6-10: severe/worst imaginable itch).[10, 11] The study population in Poland consisted of 27 women and 2 men, aged 36-75 years (average 55), and 10 women without itch, 9 women and 1 man with moderate itch, and 8 women and 1 man with severe itch. For study population in Germany, all patients were women, aged 29-64 years (average 51), and 11 patients without itch, 2 with moderate itch, and 6 with severe itch.

Study protocols were approved by the local medical institutional review boards, and all subjects provided written consent for their samples to be used. The serum supernatant was aliquoted and frozen until measurements were performed. Patients' samples were used in anonymized manner for our study without any recourse to proprietary health information.

Chemicals and antibodies

LPA 18:1, egg-LPC (LPC, mixture of LPC species 14:0, 16:0, 16:1, 18:0, 18:1, and 18:2), LPC 14:0, LPC 16:0, LPC 18:0, and LPC 18:1 were purchased from Avanti Polar Lipids (Alabaster, AL). GSK1016790A, SB366791, HC030031, capsaicin, histamine, HC067047, PF8380, U73122, resiniferatoxin, U0126, tamoxifen, 4-hydroxy tamoxifen, α-naphthyl isothiocyanate (ANIT), isopentenyl pyrophosphate (IPP), glycerophosphorylcholine phosphodiesterase, choline oxidase, peroxidase, 3-(N-Ethyl-3-methylanilino)-2-hydroxypropanesulfonic acid sodium salt (TOOS), and 4-aminoantipyrine were purchased from Sigma (St. Louis, MO). E6446 was purchased from Bocsci INC (Shirley, NY), BIM46187 was purchased from Aobious (Gloucester, MA), Gallein, GIT27, ICI 204,448 and Yoda 1 were purchased from Tocris Bioscience (Minneapolis, MN), lysophospholipase was from Sekisui Diagnostics (Burlington, MA), and GsMTx4 was from Adooq Bioscience LLC (Irvine, CA). GSK205 was synthesized by the Small Molecule Synthesis Facility at Duke University.[12] miR-146a-5p mimic (miR-146a) and miR-146a-5p negative control (scramble) were obtained from Thermo Fisher (Waltham, MA). LPA, LPCs, histamine, and GsMTx4 were dissolved in sterile normal saline (NS) and freshly made for use. miR-146a mimic and scramble were dissolved in nuclease-free water and freshly prepared before use. All other chemicals were dissolved in DMSO and further diluted until use.

Rabbit polyclonal anti-phospho-ERK, monoclonal anti-ERK, and polyclonal anti-phospho-MEK were obtained from Cell Signaling Technology (Danvers, MA). Rabbit polyclonal anti-TRPV1 was obtained from Neuromics (Edina, MN), polyclonal anti-TRPA1 from Novus Biologicals (Centennial, CO), and polyclonal anti-TRPV4 from Abcam (Cambridge, MA) from Sigma. 4′,6-diamidino-2-phenylindole (DAPI) was obtained from Sigma.

Behavioral assessment

Mice were shaved at the dorsal neck 1 d before experiments. Mice were allowed to acclimate to a Plexiglas chamber for at least 30 min before testing and received intradermal (i.d.) injection of 50 μl of LPA 18:1, LPC, LPC 14:0, LPC 16:0, LPC 18:0, LPC 18:1, miR-146a mimic, miR-146a scramble, Yoda 1 or vehicles through a 30-gauge needle (Becton Dickinson, Franklin Lakes, NJ) into the neck skin. After injections, mice were immediately placed back to the chamber, and the scratching behavior was recorded by a Panasonic video camera for 30 min. Hind limb scratching behavior directed toward the injected area at the nape of neck was observed. A scratch bout is defined as one or more rapid back-and-forth hind paw motions directed toward and contacting the treated area, ending with licking or biting of the toes or placement of the hind paw on the floor. Behavioral analysis was conducted by observers blinded to genotype.

To investigate the effects of the selective inhibitors GSK205 or HC067047 for TRPV4, SB366791 for TRPV1, HC030031 for TRPA1, PF8380 for autotaxin, U0126 for MEK, IPP for TRPV3, GIT for TLR2/6, E6446 for TLR7/9, non-selective inhibitor GsMTx4 for PIEZO 1, and selective agonist ICI 204,448 for kappa opioid receptor, on LPA-, LPC- or miR-146a-induced scratching behaviors, mice received an intraperitoneal (i.p.) injection of 0.25 ml or an intrathecal (i.t., see approach below) injection of 5 μl of chemical solutions 15 min before pruritogen injections. Control animals received the same volume of vehicles.

To test whether LPC induces scratching behavior at the spinal cord level directly, a 30-gauge needle attached to 10 μl micro-syringe (Hamilton Co., Reno, NV) was inserted between L4 and L5 segments and tail flick upon i.t injection was considered a control for targeted delivery. LPC was injected into the subarachnoid space with a total volume of 5 μl at a constant rate of 10 μl/min. Scratching behavior was recorded for 30 min and behavioral analysis was performed as described above.

To examine whether i.d. injection of LPC induces pain-like behavior in mice, a mouse cheek model was used to differentiate itch from pain.[13] In brief, 10 μl of LPC or miR-146a was administrated into the mouse cheek. Wiping (pain) and scratching (itch) behaviors were videoed for 30 min using a Panasonic camera. A bout of wiping was defined as a continuous wiping movement with a forepaw directing at the area of the injection area and a bout of scratching was defined as above.

To examine whether TRPV1-expressing sensory neurons contribute to LPC- or miR-146a-induced itch, we ablated the central terminals of TRPV1-expressing neurons by i.t. injection of 200 ng resiniferatoxin (RTX) into the L4/L5 subarachnoid space.[14] Lumbar puncture was made with a 30G-needle and drugs at 5 μl of volume were delivered. Scratching behavior assay was started approximately 2 weeks after resiniferatoxin treatment.

Scratching behaviors in monkeys were performed as previously described.[15] In brief, monkeys were seated in primate chairs and both lateral sides of upper part (i.e., the skin area over the *vastus lateralis muscle*) of their hindlimbs were shaved 1 d before experiments. The monkey's hindlimb was held by another experimenter during the injection. A 30G-needle connected with a 50 μl microsyringe (Hamilton Co., Reno, NV) was placed almost flat against skin, bevel up; and then was inserted 1/8 inch into skin. 20 μl of histamine, LPC or miR-146a solution was slowly injected and was watched for a wheal to appear. Once the injection was completed, monkeys immediately returned to his/her home cage and their potential site-specific scratching activity was recorded for 15 min after injection. A scratch was defined as one brief scraping contact of the forepaw or hind paw on the skin surface area. Scratching activities were scored by individuals who were blinded to dosing conditions. Before collecting data, monkeys had been habituated with the injection procedure and experimenter for several times. It is noted that the tested chemicals were i.d. administered to the same subjects with at least one-week interval, starting vehicle first and then chemicals in randomized doses. Based on our prior experience,

we have not observed tolerance to elicited scratching with this schedule for a well-known pruritogen histamine. In addition, this repeated injection schedule with tested chemicals did not result in any skin lesion. There was no significant difference in scratching numbers between male (n=7) and female (n=2) monkeys for tested chemicals.

Mouse model of cholestasis was induced by α-naphthyl-isothiocyanate (ANIT, dissolved in corn oil) administration via oral gavage for 5 consecutive days at 25 mg/kg. Control mice received the same volume of corn oil. Animals were habituated to the testing environment for 2 d before baseline testing. The scratching behavior was recorded by a Panasonic video camera for 1 h every day before daily ANIT treatment.

To test whether LPC induces pain behavior at the spinal cord level directly, LPC was i.t. injected into the subarachnoid space with a total volume of 5 μl at a constant rate of 10 μl/min. Mechanical pain behavior was assessed with electronic von Frey filaments (Ugo Basile, Italy). Animals were habituated to the testing environment daily for at least 2 days before baseline testing. Mice were placed on a 5×5-mm wire-mesh grid floor in individual compartments and allowed to adapt for 0.5 h prior to the von Frey test. The von Frey filament was then applied to the middle of the plantar surface of the hind paw and the withdrawal responses following the stimulation were measured 3 times and averaged. Data on mechanical threshold was express as % of change.

Cell culture and transfection

HEK293 cells (ATCC® CRL-1573) were cultured on poly-D-lysine coated coverslips in 24-well plate containing DMEM media with high-Glucose (Gibco, Gaithersburg, MD) supplemented with 10% fetal bovine serum (FBS, HyClone Laboratories, Logan, UT) and 100 U/ml of penicillin/streptomycin (Gibco, Gaithersburg, MD). Cell cultures were maintained with 5% of CO_2 in a humidified incubator at 37 °C. HEK cells were transfected with rat or human wild type or

mutant TRPV4 channels with EGFP or YFP coupled to their C-termini (1.5 µg of plasmid for excised patch clamp and Ca^{2+} imaging and 200 ng for single-channel experiments). The jetPEI™ Polyplus transfection reagent (Polyplus Transfection, New York, NY) for electrophysiology or Lipofectamine™ 2000 Reagent (Invitrogen) for Ca^{2+} imaging were used for transfections per manufacturer's instructions as previously described.[4, 16] To investigate whether miR-146a can directly activate TRPV1 channels or indirectly via TLRs, HEK293 cells were transfected with rTRPV1 or co-transfected rTRPV1 with rTLR7, rTLR2, or rTLR6 (Addgene, Watertown, MA) for Ca^{2+} imaging assay. Control cells were transfected with GFP or YFP.

Primary mouse keratinocytes were cultured following previous protocol.[5] The epidermis from the back skin of newborn WT or keratinocyte-*Trpv4* cKO mice was separated from the dermis by floating the skin on 0.25% trypsin (Gibco) for 14-18 h at 4 °C. Basal keratinocytes were separated from the cornified sheets by filtration through a 70 µM cell strainer. Keratinocytes were plated on collagen I-coated dishes or glass coverslips and grown in EME media (Gibco) containing 8% chelex (Bio-rad, Hercules, CA)-treated FBS with the final Ca^{2+} adjusted to 0.05 mM, bovine pituitary extract (50 µg/ml), epidermal growth factor (5 ng/ml), and 1x antibiotics/antimycotics (Gibco) in a humidified incubator with 5% CO_2 at 37 °C for 5-7 days until use. To knockdown *Trpv4* in isolated keratinocytes from newborn keratinocyte-*Trpv4* cKO mice, cells were treated with 4-OH tamoxifen at 500nM for 72 h.

Primary human keratinocytes were cultured as previously described.[5] In brief, surgically discarded foreskin samples, obtained from Duke Children's Hospital in accordance to institutionally approved IRB protocol, were incubated with Dispase (Gibco, 4 U/ml) for 12-16 h at 4°C followed by 0.05% trypsin (Gibco) for 10-20 min at 37°C. Cells were maintained in keratinocyte serum-free media (Invitrogen) with 5% CO_2 at 37°C and used at passage 2-3.

Primary mouse sensory neurons were cultured following previous protocol.[4] DRGs from 2-3 weeks old male WT, *Trpv1* KO, and *Trpa1* KO mice were dissected and digested with 1 mg/mL collagenase (Worthington, CSL1) and 5 mg/mL dispase (Invitrogen) for 1 h, then triturated. The resulting cell suspension was filtered through a 70 μm cell strainer (BD Biosciences, Bedford, MA) to remove debris. Neurons were cultured in DH10 medium (1:1 DMEM:Hams-F12, Invitrogen) with 10% FBS (Sigma), 100 U/mL penicillin and 100 μg/mL streptomycin (Gibco) and 50 ng/mL nerve growth factor (NGF; USBiological) on coverslips coated with poly-D-lysine and laminin (Invitrogen), and incubated with 5% CO_2 at 37 °C. Ca^{2+} imaging was performed next day after culture.

Modeling of LPC binding to TRPV4 channels

The TRPV4 structure from *Xenopus tropicalis* (PDB file 6BBj, [17]) was used within the Schrodinger software package. Within Schrodinger, the protein preparation wizard within the Maestro Molecular Modeling Interface was run, and a conformer library of LPC 18:1, was generated using the ligand preparation tool. Within the Schrodinger software tool, the TRPV4 protein structure was minimized using the optimized potentials for liquid simulations model force field with standard parameters (OPLS, version 3e).[18] The receptor grid generation was centered on residue K750 using the maximum 36 Angstrom distance. Ligand-receptor docking was performed using the Glide software platform. [19]

Site-directed mutagenesis of TRPV4 channels

TRPV4 sequences of multiple species were aligned using Clustal Omega program. Site-directed mutagenesis to generate point mutations in rat and human TRPV4 channels were carried out

using Phusion DNA polymerase enzyme [20-22], with final sequencing to check for presence of the induced mutation. We introduced the following mutations into the rTRPV4 or hTRPV4 channel: R746C, R746G, R746D, K754G, R757G, R774G, and W776G.

In vitro and ex vivo Ca^{2+} imaging

Routine procedures were followed for Ca^{2+} imaging in cultured DRG sensory neurons, epidermal keratinocytes, and HEK cells.[4, 5] Ca^{2+} imaging of cultured cells in response to chemical solutions was conducted after loading with 5 μM Fura2-AM (Invitrogen) for 45 min following a ratiometric Ca^{2+}-imaging protocol with 340/380-nm blue light for dual excitation. Ratios of emissions were acquired at 0.5 Hz. $\Delta R/R_0$ was determined as the fraction of the increase of a given ratio over baseline ratio divided by baseline ratio. To investigate the effects of the TRPV4 inhibitors GSK205 or HC067047, the PLC inhibitor U73122, the $G\alpha_q$ G Protein inhibitor BIM46187, the $G\beta\gamma$ G protein inhibitor Gallein, the TRPV1 inhibitor SB366791, the TRPA1 inhibitor HC030031, the TRPV3 inhibitor IPP, the PIEZO 1 inhibitor GsMTx4, on LPA-, LPC-, miR-146a, or Yoda 1-induced Ca^{2+} influx, cells were incubated with the inhibitors for 15 min before stimulation. Control cells received vehicles.

A previously established method was followed for *ex vivo* Ca^{2+} imaging of DRG explants.[2] Intact DRGs (L4 or L5) were isolated from naïve male or female Pirt-GCaMP3 mice (2-3 months old) and equilibrated in artificial cerebrospinal fluid (ACSF) bubbled with 95% O_2/5% CO_2 at room temperature. After 15 min, explants were placed in a dish with 2 ml of pre-oxygenated ACSF and imaged using a Zeiss 780 upright confocal microscope (Carl Zeiss AG, Oberkochen, Germany) with 20x water immersion objective and Z-stack approach at the 488 nm wavelength. Explants were stimulated by miR-146a or miR-146a scramble. After 15 min recording, capsaicin was then applied to identify whether the miR-146a responding

neurons were TRPV1 positive. In addition, to examine whether inhibition of TRPV1 or TRPA1 ion channels attenuates miR-146a-induced Ca^{2+} signal, explants were pretreated with the TRPV1 inhibitor SB366791 or the TRPA1 inhibitor HC030031 during the 15 min sample equilibration. Ca^{2+} fluorescence intensity was determined using the ImageJ software (NIH, Bethesda, MD, USA). For each neuron, the pixel intensity (F_t) was assessed for each frame and the pixel intensity recorded from the first 20 frames was taken to determine the average baseline value (F_0). Ca2+ signal amplitudes are presented as $\Delta F/F_0$, which is the ratio of fluorescence difference (F_t-F_0) to baseline (F_0).

Electrophysiology

Currents were recorded using the inside-out configuration of the patch-clamp technique.[23] Solutions were changed with a RSC-200 rapid solution changer (Molecular Kinetics). GSK1016790A was prepared in DMSO at 15.25 mM for the stock, which was kept at -20 ºC and diluted to 1 µM in recording solution for application to membrane patches. LPC 18:1 was prepared in DMEM-BSA 0.1% at 10 mM for stock solutions, kept at -70 ºC and diluted in recording solution. The recording solutions contained (in mM): 130 NaCl, 3 HEPES (pH 7.2) and 1 EDTA for the bath and 130 NaCl, 3 HEPES (pH 7.2) and 5 $CaCl_2$ in the pipette. Experiments were performed at room temperature. Mean current values in response to GSK1016790A or LPC 18:1 were measured after channel activation had reached the steady-state (~3 min). Currents were obtained using voltage protocols where the holding potential was 0 mV and 10 mV steps from -120 to 120 mV or from -60 to +60 mV for 100 ms, to 0 mV. Borosilicate glass was used for pipette fabrication (5 MΩ). Currents were low-pass filtered at 2 kHz and sampled at 10 kHz with an EPC 10 amplifier (HEKA Elektronik) and were plotted and analyzed with Igor Pro (Wavemetrics Inc.).

For single-channel recordings, Borosilicate glass 30 MΩ pipettes were used. Recordings were obtained at +60mV by acquiring several traces of 1-3s duration. The effect of GSK1016790A or LPC 18:1 on single TRPV4 channels was studied in inside-out. Currents were filtered at 2 kHz and sampled at 5 kHz. Patches containing only one channel activated by different compounds were identified as those that did not contain overlapping opening events. Single-channel openings and closures were identified with the half-threshold crossing technique.[16] The channel open probability was calculated as the sum of the total open time divided by the sweep duration. Dwell times and amplitude histograms in the closed or open states were collected in logarithmic time histograms according to the Sine-Sigworth transformation.[24] Sums of three or two exponential components were fitted to histograms using a least-squares algorithm.

In vitro interaction assays of LPC-TRPV4

Surface proteins were obtained from HEK293 cells transiently expressing rTRPV4-EGFP channels using the Pierce Cell Surface Isolation kit (Pierce Biotechnology, Rockford, IL) following the manufacturer's instructions. Overlay assays were performed as previously described.[16] In brief, LPC 18:1 was spotted (200 pmol per spot) onto a nitrocellulose membrane (GE Healthcare, Pittsburgh, PA) and then blocked with 1% fatty acid-free BSA (Calbiochem) and 6% fat-free dried milk in PBS. Membranes were then incubated with the surface protein solutions and exposed to anti-GFP antibody (Sigma) diluted 1:1000 in 3% fat-free dried milk in PBST (with 0.1% of Tween). Membranes were incubated with horseradish peroxidase-conjugated secondary anti-rabbit antibody (Cell Signaling Technology) diluted 1:7500 in 6% fat-free dried milk in PBST. The binding of rTRPV4-EGFP and TRPV4-R746D-EGFP to the lipid-containing spots was visualized by chemiluminescence by exposing the blot for 15 min (Amersham Bioscience, Piscataway, NJ). Semi-quantitative densitometric analysis was done using ImageJ (NIH) and expressed as relative protein levels of TRPV4 bound to each spot.

Western Blot

Routine procedures were followed.[4, 5] Briefly, cultured keratinocytes and dissected dorsal neck skin (0.5×0.5 cm, the area that received the treatment) were protein-extracted in radioimmunoprecipitation assay (RIPA, Sigma) buffer and electroblotted to polyvinylidene fluoride (PVDF) membranes after gel separation of proteins in a 4-15% polyacrylamide gel (Bio-Rad). Membranes were blocked with 5% BSA in TBST, and incubated with primary antibodies rabbit anti-pERK or anti-ERK (both at 1:2000) followed by secondary antibody (anti-rabbit peroxidase-conjugated, 1:5000; Jackson ImmunoResearch), and chemiluminescence substrate (ECL-Advance, GE Healthcare). Immunoblot band intensity was quantitated using the software Image J and ERK served as a control for pERK expression.

Immunohistochemistry and morphometry analysis

Routine procedures were followed.[4] Briefly, mice were perfused transcardially with 0.01 M PBS followed by ice-cold 4% paraformaldehyde (PFA, Sigma). Cervical spinal cord, TGs and cervical DRGs, and dorsal neck skin were dissected and post-fixed in 4% PFA overnight, cryoprotected in 20% sucrose (48 h) and sectioned on a cryostat (30 µm for spinal cord, 12 µm for TG and DRG and neck skin). Sections were blocked with 5% normal goat serum (Jackson), and incubated overnight with primary antibodies: rabbit anti-TRPV1 (1:5000), TRPA1 (1:200), TRPV4 (1:300) or p-MEK (1:200). Immunodetection was accomplished with secondary antibodies (AlexaFluor 594-conjugated goat anti-rabbit) for 2h, and cover-slipped with Vectashield (Vector). DAPI (1 µg/ml) was used for counterstaining with p-MEK in skin sections. Digital micrographs were acquired using a BX61 Olympus upright microscope with a high-resolution ORCA-Spark camera (Hamamatsu) and with constant acquisition/ exposure settings, using CellSens Dimension software (Olympus). 4-6 sections were analyzed per mouse. TG and DRG neurons were identified by morphology. The cutoff density threshold was determined by averaging the density of three neurons per section that were judged to be minimally positive,

using ImageJ software. All neurons for which the mean density exceeded the threshold >25% were judged as positive. Positive cells were expressed as % of total counted TG neurons. The labeling density of TRPV1 in spinal cord was measured using the integrated density algorithm of Image J.

Measurement of released vesicles and extracellular miR-146a from cultured keratinocytes or sera

Medium for the cultured keratinocytes was replaced with serum-free medium 2 h before LPC stimulation. Fifteen minutes after LPC, the supernatant of the cells was harvested and subjected to two steps of centrifugation (i) 300 g for 5 min to eliminate remaining cells, (ii) 16,000 g for 30 min to eliminate cell debris and apoptotic bodies. Finally, cell-free supernatants were further purified using a Vesicular Isolation kit (Invitrogen) according to the manufacturer's instructions, with final product resuspended in ice-cold PBS. Total RNA extraction was then carried out using a Total RNA Isolation kit (Invitrogen). Enrichment for small RNAs was carried out by sequential increase in ethanol concentration and passing through glass-fiber filters. RNase free water was used to elute small RNAs in the final elution step. For human PBC sera or sera from ANIT-treated mice, RNA was isolated using Qiagen miRNeasy Plasma/Serum kit. cDNA synthesis from extracted RNAs was performed according to manufacturer's instructions (qSTAR miRNA kit, Origene). For qPCR, the stem-loop oligonucleotides specific for the following miRs are as follows: miR-146a-5p (GAGAACTGAATTCCATGGG), miR-let-7b (GAGGTAGTAGGTTGTGTGG), miR-125b-1 (CCCT GAGACCCTAACTTG), miR-203 (GTGGTTC TTGACAGTTCAAC), and miR-16-5p (AGCAGCAC GTAAATATTGGC). Primers were purchased from Integrated DNA Technologies company. qPCR reactions for each sample were run in triplicates, including no-template controls. MiR-16-5p was selected as a control due to the relative constancy of its expression in various cultured cell lines.[25] qPCR for this miR was

performed in tandem with target miRs to determine the optimal normalization procedure. To investigate the effects of the specific TRPV4 inhibitors GSK205 or HC067047 and the specific MEK inhibitor U0126 on LPC-induced extracellular release of miR-146a, cells were incubated with the inhibitors for 15 min before stimulation. Control cells received the same volume of vehicle.

Vesicular release from cultured keratinocytes was quantified by detecting acetylcholinesterase (AChE) activity in the extracellular release fluid. [26, 27] CBQCA Protein Quantitation Kit (Molecular Probes, Eugene, OR) was used to assess the total protein amounts of each sample. Quantitation was carried out according to kit instructions (Fluorocet, Systems Biosciences, Palo Alto, CA). Briefly, vesicles were lysed to release esterase enzyme whose activity is measured using a florescence dye, excitation at 544 nm and emission at 590 nm. Fluostar Optima (BMG Labtech, Cary, NC) microplate reader was used to measure esterase activity. 500ng protein equivalent of input was used per well. To determine the contribution of Rab5a and Rab27a to LPC-induced miR-146a release, cells were pre-treated with the Rab5a (5'-GUAGAAUCAA GUUUCUAAUUCUGAA-3', 5'-UUCAGAAUUAGAAACUUGAUUCUACCA-3') or Rab27a (5'-AGCUAAAA CUGAGAGCUUCAAACAG-3', 5'-CUGUUUGAAGCUCUCAGUUUUAGCUUA-3') siRNA (IDT, Coralville, IA) for 72h before stimulation. Control cells were treated with scramble siRNA.

LPC measurement in sera and skin

Blood and dorsal neck skin (~ 0.5 x0.5 cm) were harvested from ANIT- or control-treated mice at day 5. Blood was drawn via cardiac puncture and allowed to clot at room temperature for 20 min. After centrifugation at 2000xg for 10 min at 4°C, serum was collected and stored at -80 °C until use. After weighing, skin was cut into pieces and sonicated in methanol for 1 min at 4°C.

After sonication, samples were centrifuged at 12000xg for 15min at 4°C and supernatant was collected and stored at -80 °C until analysis. Total levels of LPC in mouse serum and skin were determined by an enzymatic colorimetric method.[28] In brief, 8 µl of samples were treated with lysophospholipase, glycerophosphorylcholine, phosphodiesterase, and choline oxidase. The resulting hydrogen peroxide generated was quantified using horseradish peroxidase and TOOS reagent. The absorbance was measured by microplate reader (Molecular Devices, San Jose, CA). Total level of LPC was detected at around 1 mM in sera of control mice. Total levels of LPC in serum of no-liver-disease controls (~218 µM) and PBC patients from Duke Gastroenterology-Hepatology outpatient program, non-alcoholic fatty liver disease (NAFLD) clinical research program were also determined by this enzymatic colorimetric method as described above.

Serum levels of LPC in PBC patients from two clinical sites, Liver and Internal Medicine Unit of the Warsaw Medical University, Poland, and Department of Medicine 1, Gastroenterology, Hepatology, Pneumology and Endocrinology of the University Hospital of Erlangen, Germany, were determined by the AbsoluteIDQ™ p180 kit (Biocrates, Life Sciences AG, Innsbruck, Austria) following the manufacturer's instructions. The assay allows simultaneous quantification of 188 metabolites out of 10 µl serum, including 14 species of LPC: 14:0, 16:0, 16:1, 17:0, 18:0, 18:1, 18:2, 20:3, 20:4, 24:0, 26:0, 26:1, 28:0, and 28:1. In brief, after 10 µl internal standards or 10 µl serum were added into the filter wells of a 96-well plate, the wells were dried by nitrogen, and 50 µl of 5% phenyl-isothiocyanate solution was added into each well for derivatization. After incubation, the wells were dried again, and 300 µl of methanol containing 5 mM ammonium acetate were added into each well to extract the metabolites. The extract was then centrifuged into the collection wells, and each well was diluted with 300 µl of the running solvent (a proprietary mixture provided by Biocrates). The flow injection analysis-tandem mass spectrometry (FIA-MS/MS) technique was used to detect 14 species of LPC. Using electrospray

ionization in positive mode, samples were introduced directly into a Xevo TQ-S triple quadrupole mass spectrometer (Waters) operating in the Multiple Reaction Monitoring (MRM) mode. MRM transitions (compound-specific precursor to product ion transitions) for each analyte and internal standard were collected over the appropriate retention time. The FIA-MS/MS data were analyzed using Biocrates MetIDQ™ software. Internal standards and quality control samples of the p180 Kit were utilized to benchmark the quality of the assay and the robustness of the data. For all analyzed LPC species, data were expressed in relative concentrations. Of note, LPC 14:0 data was not shown since it was below the lower limit of detection. Total level of 14 LPC species as above was detected at around 155 μM in sera of PBC patients without itch.

Quantitative real-time PCR

Total RNA from TGs or cervical DRGs was prepared using Directzol RNA kit (Zymo Research) following the manufacturer's instructions. RNA was aliquoted and stored at -80 °C until use. 1 μg of total RNA was reverse transcribed using SuperScript III Reverse Transcriptase (Invitrogen). Real-time PCR was performed with equal amounts of cDNA in the GeneAmp 7700 sequence detection system (Applied Biosystems) using QuantiTect SYBR Green PCR Kit (Qiagen). The ΔΔCt method was used for relative quantification of gene expression. Primers were synthesized by Integrated DNA Technologies and their sequences are: internal control ß-tubulin (forward: 5'-CCTG CCTTTTCGTCTCTAGC CGC-3', reverse: 5'-GCTGATGACCTCCCA GAACTTGGC-3') and TRPV4 (forward: 5'-GTGGGCAAGAGCTCAGATGGCACTC-3', reverse: 5'-CCACCGAGG ACCAACGATCCCTAC G-3').

Supplementary References

1. Liedtke W, Tobin DM, Bargmann CI, et al. Mammalian TRPV4 (VR-OAC) directs behavioral responses to osmotic and mechanical stimuli in Caenorhabditis elegans. Proc Natl Acad Sci U S A 2003;100 Suppl 2:14531-6.
2. **Kim YS**, **Chu Y**, Han L, et al. Central terminal sensitization of TRPV1 by descending serotonergic facilitation modulates chronic pain. Neuron 2014;81:873-887.
3. Moore C, Cevikbas F, Pasolli HA, et al. UVB radiation generates sunburn pain and affects skin by activating epidermal TRPV4 ion channels and triggering endothelin-1 signaling. Proc Natl Acad Sci U S A 2013;110:E3225-34.
4. Chen Y, Kanju P, Fang Q, et al. TRPV4 is necessary for trigeminal irritant pain and functions as a cellular formalin receptor. Pain 2014;155:2662-72.
5. Chen Y, Fang Q, Wang Z, et al. Transient Receptor Potential Vanilloid 4 Ion Channel Functions as a Pruriceptor in Epidermal Keratinocytes to Evoke Histaminergic Itch. J Biol Chem 2016;291:10252-62.
6. Agarwal N, Offermanns S, Kuner R. Conditional gene deletion in primary nociceptive neurons of trigeminal ganglia and dorsal root ganglia. Genesis 2004;38:122-9.
7. **Dankort D**, **Curley DP**, Cartlidge RA, et al. Braf(V600E) cooperates with Pten loss to induce metastatic melanoma. Nat Genet 2009;41:544-52.
8. **Van Keymeulen A**, **Rocha AS**, Ousset M, et al. Distinct stem cells contribute to mammary gland development and maintenance. Nature 2011;479:189-93.
9. EASL Clinical Practice Guidelines: The diagnosis and management of patients with primary biliary cholangitis. J Hepatol 2017;67:145-172.
10. Jacoby A, Rannard A, Buck D, et al. Development, validation, and evaluation of the PBC-40, a disease specific health related quality of life measure for primary biliary cirrhosis. Gut 2005;54:1622-9.
11. Raszeja-Wyszomirska J, Wunsch E, Krawczyk M, et al. Assessment of health related quality of life in polish patients with primary biliary cirrhosis. Clin Res Hepatol Gastroenterol 2016;40:471-9.
12. Kanju P, Chen Y, Lee W, et al. Small molecule dual-inhibitors of TRPV4 and TRPA1 for attenuation of inflammation and pain. Sci Rep 2016;6:26894.
13. Shimada SG, LaMotte RH. Behavioral differentiation between itch and pain in mouse. Pain 2008;139:681-7.
14. Mishra SK, Hoon MA. Ablation of TrpV1 neurons reveals their selective role in thermal pain sensation. Mol Cell Neurosci 2010;43:157-63.
15. Lee H, Ko MC. Distinct functions of opioid-related peptides and gastrin-releasing peptide in regulating itch and pain in the spinal cord of primates. Sci Rep 2015;5:11676.
16. Morales-Lázaro SL, Llorente I, Sierra-Ramírez F, et al. Inhibition of TRPV1 channels by a naturally occurring omega-9 fatty acid reduces pain and itch. Nat Commun 2016;7:13092.
17. Deng Z, Paknejad N, Maksaev G, et al. Cryo-EM and X-ray structures of TRPV4 reveal insight into ion permeation and gating mechanisms. Nat Struct Mol Biol 2018;25:252-260.
18. Harder E, Damm W, Maple J, et al. OPLS3: A Force Field Providing Broad Coverage of Drug-like Small Molecules and Proteins. J Chem Theory Comput 2016;12:281-96.
19. Friesner RA, Banks JL, Murphy RB, et al. Glide: a new approach for rapid, accurate docking and scoring. 1. Method and assessment of docking accuracy. J Med Chem 2004;47:1739-49.
20. **Salazar H**, **Jara-Oseguera A**, **Hernandez-Garcia E**, et al. Structural determinants of gating in the TRPV1 channel. Nat Struct Mol Biol 2009;16:704-10.

21. Rosenbaum T, Gordon SE. Dissecting intersubunit contacts in cyclic nucleotide-gated ion channels. Neuron 2002;33:703-13.
22. Hsieh PC, Vaisvila R. Protein engineering: single or multiple site-directed mutagenesis. Methods Mol Biol 2013;978:173-86.
23. Hamill OP, Marty A, Neher E, et al. Improved patch-clamp techniques for high-resolution current recording from cells and cell-free membrane patches. Pflugers Arch 1981;391:85-100.
24. Sigworth FJ, Sine SM. Data transformations for improved display and fitting of single-channel dwell time histograms. Biophys J 1987;52:1047-54.
25. **Schwarzenbach H**, **da Silva AM**, Calin G, et al. Data Normalization Strategies for MicroRNA Quantification. Clin Chem 2015;61:1333-42.
26. Gupta S, Knowlton AA. HSP60 trafficking in adult cardiac myocytes: role of the exosomal pathway. Am J Physiol Heart Circ Physiol 2007;292:H3052-6.
27. Malik ZA, Liu TT, Knowlton AA. Cardiac Myocyte Exosome Isolation. Methods Mol Biol 2016;1448:237-48.
28. Kishimoto T, Soda Y, Matsuyama Y, et al. An enzymatic assay for lysophosphatidylcholine concentration in human serum and plasma. Clin Biochem 2002;35:411-6.

(Author names in bold designate shared co-first authorship)

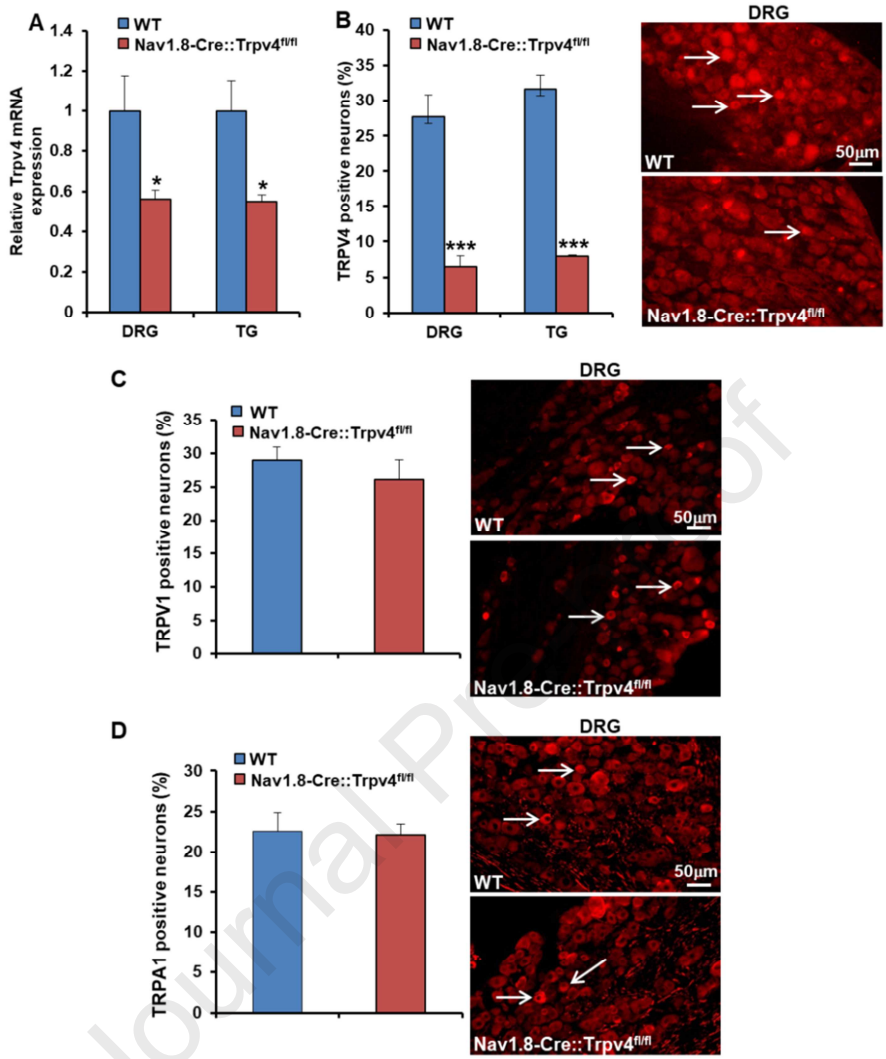

Supplementary Figure 1. Depletion of *Trpv4* mRNA and protein in dorsal root ganglion (DRG) and trigeminal ganglion (TG) of Nav1.8-Cre::Trpv4$^{fl/fl}$ mice.

(*A*) qRT-PCR shows that *Trpv4* mRNA was significantly reduced in Nav1.8-Cre::Trpv4$^{fl/fl}$ mice. *p<0.05 vs WT, two-tailed t-test, n=4-5 mice/group.

(*B-D*) Immunostaining with their respective, specific antibodies shows reduced TRPV4-(B), but unchanged TRPV1(C)- or TRPA1(D)-expressing neurons, in Nav1.8-Cre::Trpv4$^{fl/fl}$ mice. Arrows represent TRP-positive neurons. ***p<0.001 vs WT, two-tailed t-test, n=4 mice/group (>1200 total neurons counted/group).

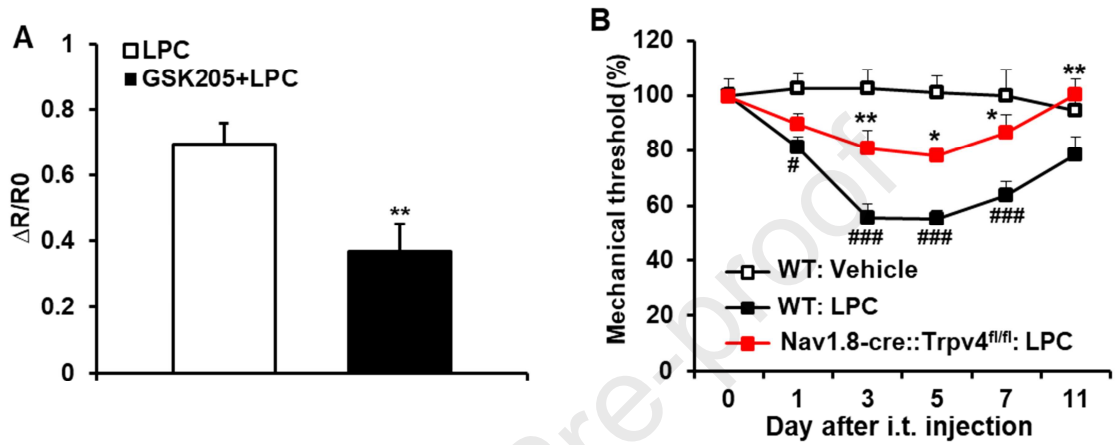

Supplementary Figure 2. Intrathecal (i.t.) injection of LPC induces mechanical pain via activation of TRPV4-expressing dorsal root ganglion (DRG) sensory neurons.

(*A*). Inhibition of TRPV4 with its selective inhibitor GSK205 (10 μM) reduced LPC (10 μM)-induced Ca^{2+} signal in cultured DRG neurons. **p<0.01 vs. LPC, two-tailed t test. N≥250 cells recorded/treatment.

(*B*). Single i.t. injection of LPC (15 μg/5 μl) induced long-lasting pain, as evidenced by reduced mechanical withdrawal thresholds. Pain behavior was attenuated in sensory neuron-*Trpv4* cKO (Nav1.8-Cre::$Trpv4^{fl/fl}$) . $^{\#}$p<0.05 and $^{\#\#\#}$p<0.001 vs. WT: Vehicle (normal saline), and *p<0.05 and **p<0.01 vs. WT: LPC, two-way ANOVA with Tukey's post-hoc test. N=7-8 mice/group.

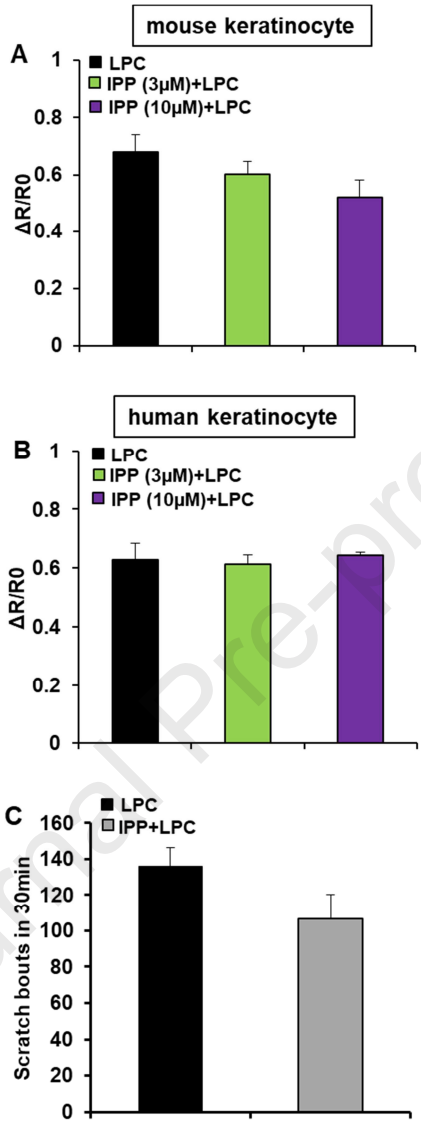

Supplementary Figure 3. Keratinocyte-TRPV3 is not involved in LPC-induced itch.

(*A*-*B*): LPC (10 μM)-induced Ca^{2+} signal in cultured mouse (A) or human (B) keratinocytes was not significantly influenced by inhibition of TRPV3 with selective inhibitor IPP. One-way ANOVA with Tukey's post-hoc test, n≥180 cells recorded/treatment.

(*C*): i.d. injection of LPC (500μg)-induced itch was not significantly attenuated in mice pre-treated with TRPV3 inhibitor IPP (10 mg/kg, i.p.). Two-tailed t test. N=13 mice for LPC and 5 for IPP+LPC.

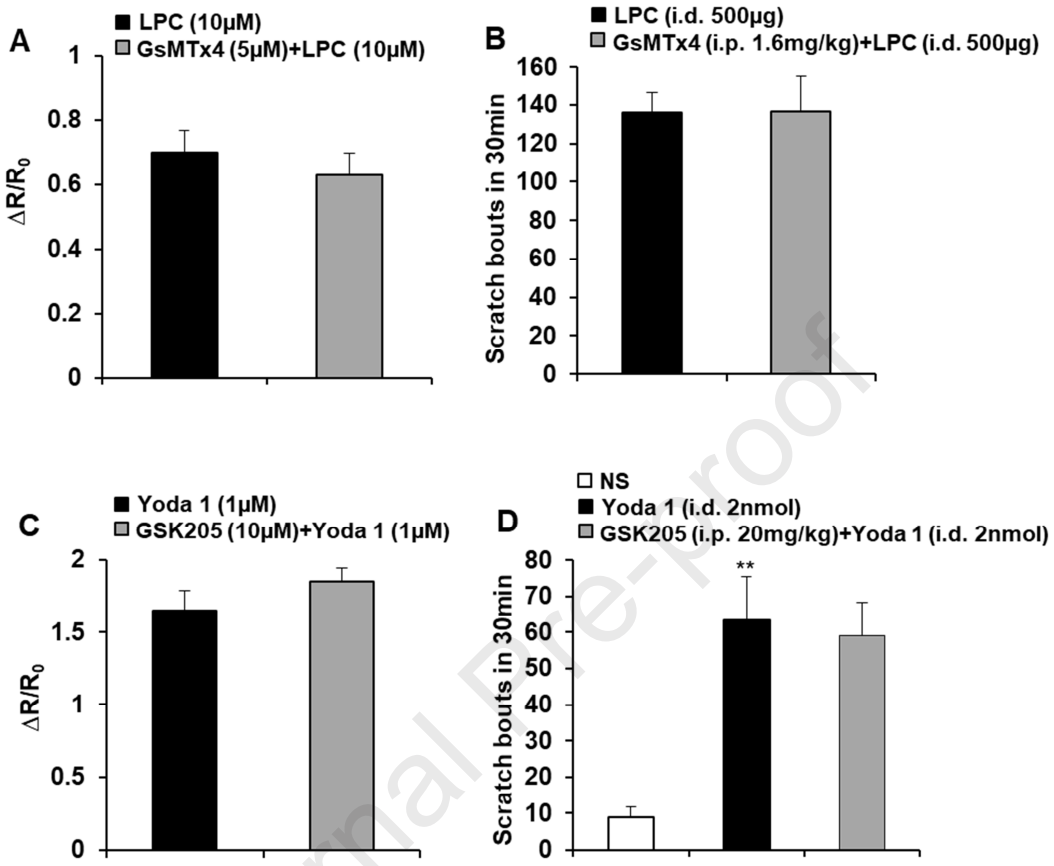

Supplementary Figure 4. Piezo-1 is not involved in LPC-TRPV4-induced itch.

(*A-B*): LPC-induced Ca^{2+} signal in cultured mouse keratinocytes (A) and scratching behavior (B) were not significantly influenced by PIEZO-1 inhibitor GsMTx4. Two-tailed t test, n≥180 cells recorded/treatment (A) and n=13 mice for LPC and 5 for GsMTx4+LPC (B).

(*C-D*): Activation of Piezo-1 with the selective agonist Yoda 1 caused Ca^{2+} signal in cultured mouse keratinocytes (C) and scratching behavior (D), which were not significantly affected by pretreatment with TRPV4 selective inhibitor GSK205. Two-tailed t test, n≥188 cells recorded/treatment (C) and One-way ANOVA with Tukey's post-hoc test, n=4-5 mice/group, **p<0.01 vs NS (normal saline) (D).

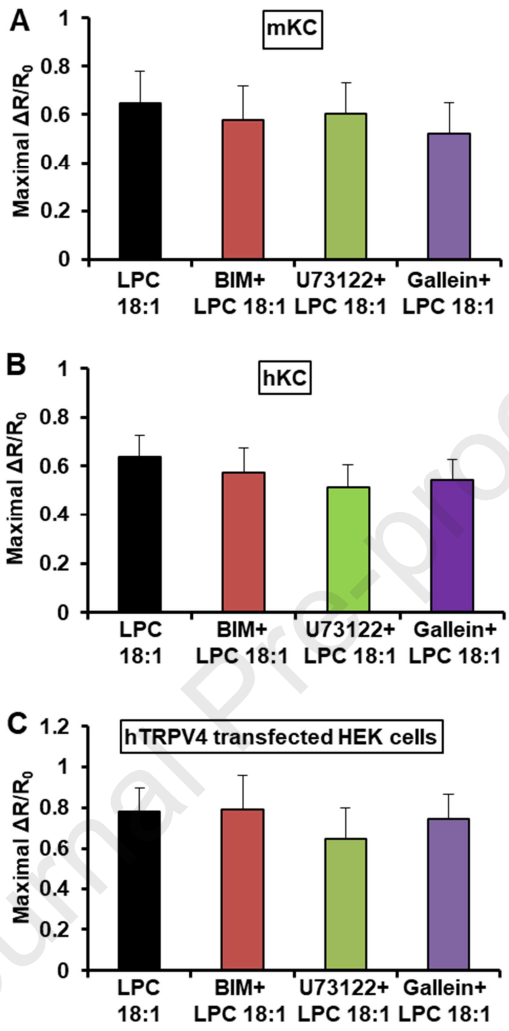

Supplementary Figure 5. Lack of evidence for GPCR-signaling upstream of TRPV4 in Ca^{2+} influx.

Ca^{2+} influx in cultured mouse (*A*) and human (*B*) keratinocytes (KC) and in HEK cells transfected with hTRPV4 (*C*), induced by LPC 18:1 (10 µM), was not significantly altered by $G\alpha_q$ inhibitor BIM46187 (BIM), phospholipase C inhibitor U73122, or $G\beta\gamma$ inhibitor Gallein (all at 10 µM). One-way ANOVA with Tukey's post-hoc test. n≥140 cells recorded/treatment.

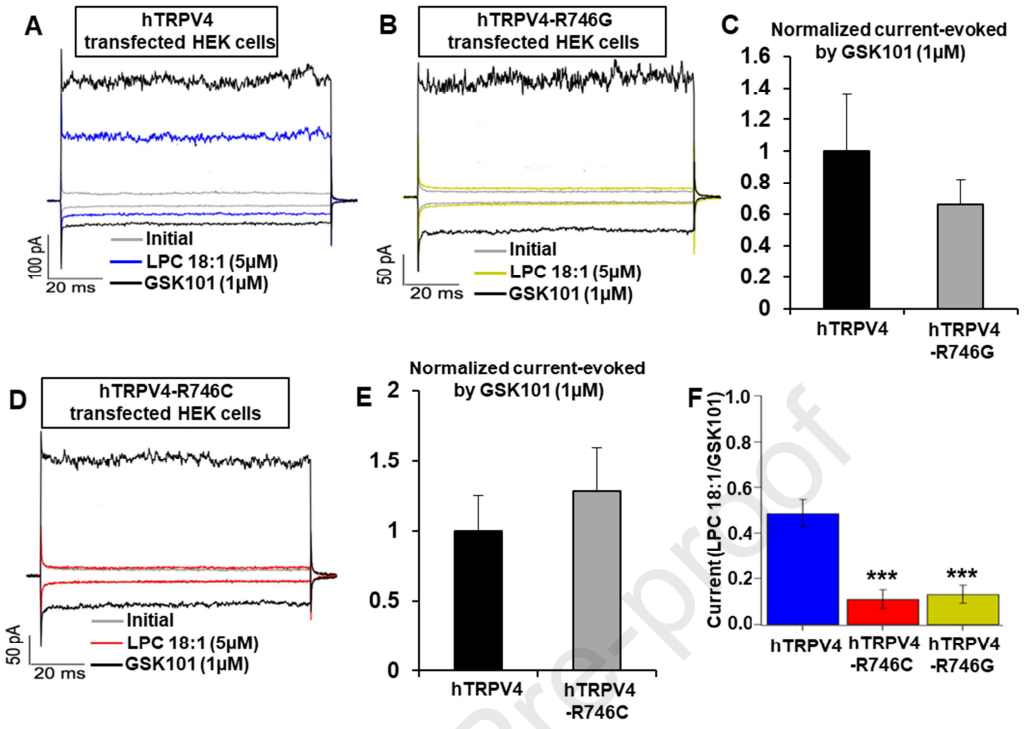

Supplementary Figure 6. Electrophysiology findings of hTRPV4 with mutations at R746 reiterate its critical relevance for channel activation by LPC 18:1

(*A-E*) Representative currents for hTRPV4 (A), hTRPV4-R746G (B), and hTRPV4-R746C (D) channels: Currents were recorded in the absence of agonist (grey), in the presence of 5 μM LPC 18:1 (blue, yellow and red, respectively) or in the presence of 1 μM GSK101 (black) at -60 and 60 mV. (C) Inert glycine mutation R746G of hTRPV4 responds to chemical activation with GSK101. Note lack of significant differences between groups, two-tailed t test, n=4 cells recorded for TRPV4(WT), left-hand black bars, average current pegged to "1", n=5 cells for TRPV4(R746G), right-hand grey bars. (E) Human genomic polymorphism mutation R746C of hTRPV4 responds to chemical activation with GSK101. Note lack of significant differences between groups, twp-tailed t-test, n=9 cells recorded for both channel isoforms; TRPV4(WT), left-hand black bars, average current pegged to "1", TRPV4(R746C), right-hand grey bars.

(*F*) There was a significant reduction of currents in hTRPV4-R746C or hTRPV4-R746G transfected HEK cells when activating with 5 µM LPC 18:1 (average activation was 48 ± 6% for WT-hTRPV4, 11 ± 4% for hTRPV4-R746C, and 13 ± 4% for hTRPV4-R746G). Data were normalized to activation obtained with 1 µM GSK101. ***p<0.001 vs. hTRPV4, One-way ANOVA with Tukey's post-hoc test. N=5-10 cells/condition.

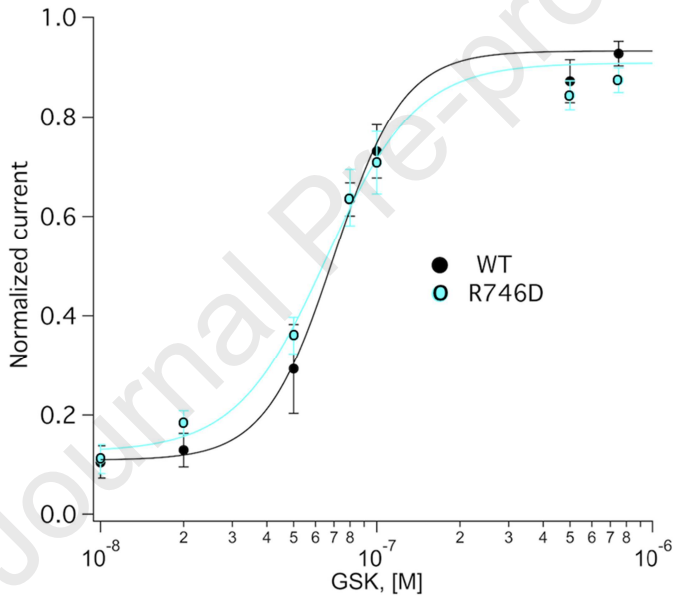

Supplementary Figure 7. Dose-response curve for activation with GSK101 at +100 mV in the inside-out configuration for rTRPV4 (WT, filled symbols, black) vs rTRPV4 (R746D, empty symbols, turquoise) transfected HEK cells. Note that there was no significant difference between WT and the R746D mutant. Smooth curve is a fit with the Hill equation (rTRPV4(WT) EC_{50}=70nM and Hill coefficient=3.2; rTRPV4(R746D) EC_{50}=66nM and Hill coefficient=2.6). Due to seal instability a single GSK101 concentration was tested per membrane-patch and the current was normalized to the current activated with 1µM GSK101 in the same patch. Group data are represented as mean±SEM of 4-9 patches per concentration.

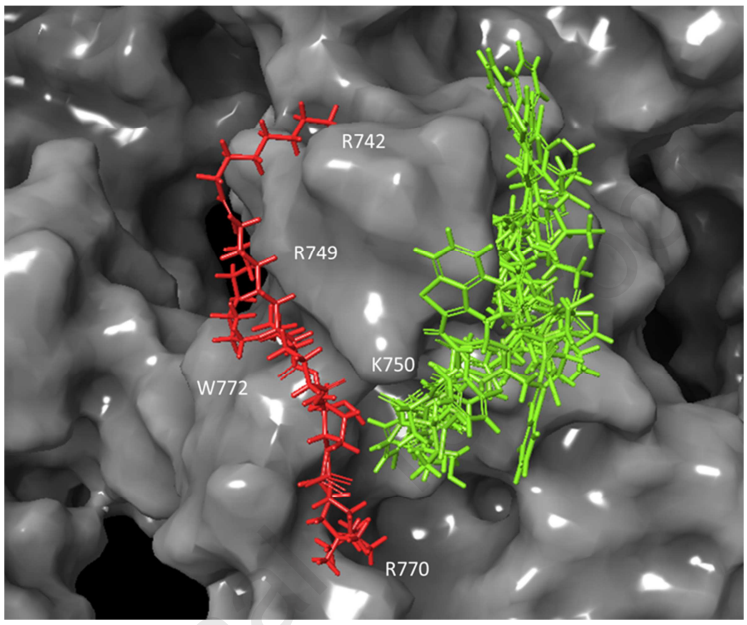

Supplementary Figure 8. Overlay of all the predicted conformer binding poses of LPC 18:1 (left, red) and GSK 101 (right, green) relative to highlighted residues of xenopus TRPV4.

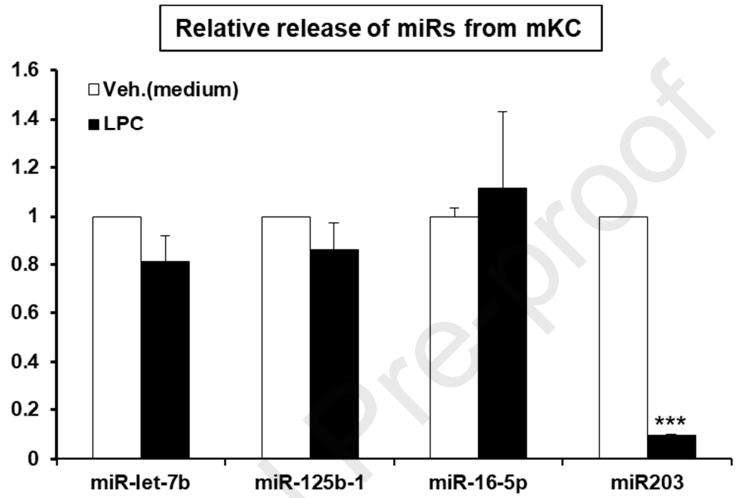

Supplementary Figure 9. LPC stimulation (10 µm, 15min) did not increase the extracellular release of miR-let-7b, miR-125b-1, miR-16-5p, or miR-203 from cultured mouse keratinocytes (KC). **p<0.001 vs. Veh. (medium), two tailed t -test was used. N=3 cultures/group (5-7 pups/culture).

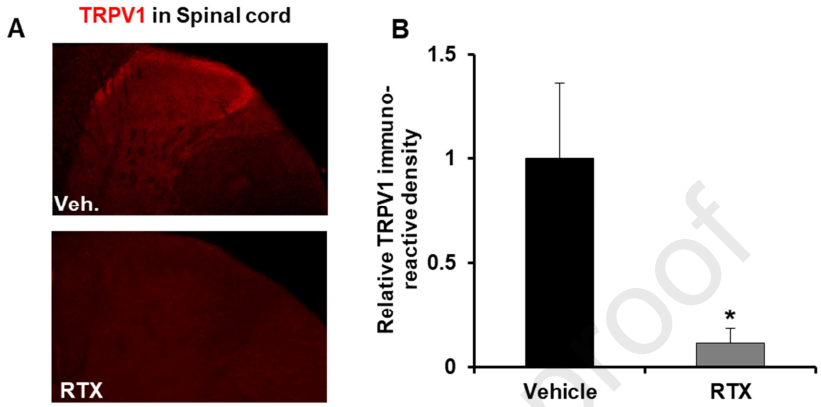

Supplementary Figure 10. Elimination of TRPV1^{+} central nerve terminals in superficial layers of the spinal cord by i.t. injection of resiniferatoxin (RTX).

(*A*) Immunolabeling of TRPV1 in spinal cord of Veh. (5% DMSO+5% Tween80)- or RTX (200 ng/5µl)-treated mice.

(*B*) Quantification of TRPV1 immuno-reactive nerve terminals in superficial layers of spinal cord dorsal horn. $^{*}p<0.05$ vs. Veh., two tail t-test, n=4-5 mice/group.

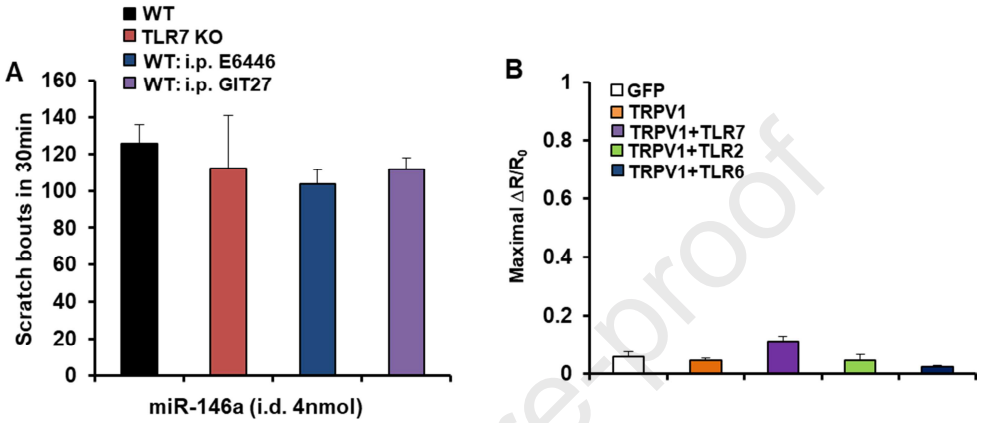

Supplementary Figure 11. Lack of evidence of direct activation of TRPV1 or TLRs signaling upstream of TRPV1 in response to miR-146a.

(*A*). Mouse scratching behavior evoked by i.d. injection of miR-146a (4 nmol) was not significantly altered by knockout of Tlr7, i.p. treatment with TLR7/9 inhibitor E6446 or TLR2/6 inhibitor (GIT27) at 10 mg/kg. One-way ANOVA with Tukey's post-hoc test. N=4-7/group.

(*B*). HEK293 cells transfected with rTRPV1 or co-transfected with rTRPV1 and rTLRs did not show a significant Ca2+ transient upon stimulation with miR-146a at 300 nM when compared to control (GFP-transfected). One-way ANOVA with Tukey's post-hoc test. N≥260 cells /group.

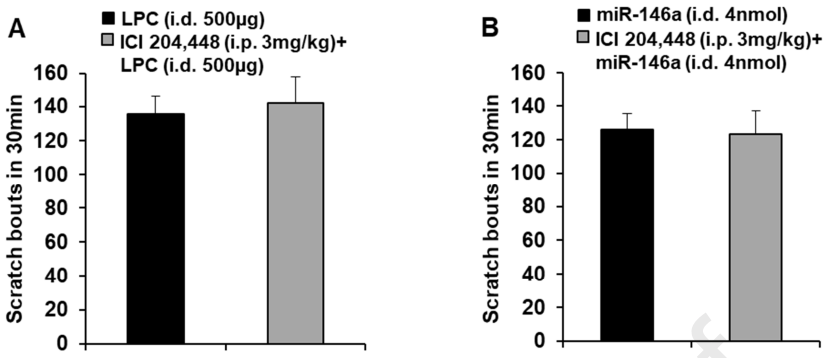

Supplementary Figure. 12. Kappa-opioid-receptor (KOR) is not involved in LPC- or miR-146a-induced itch. LPC- (A) or miR-146a (B)-induced scratching behavior was not significantly affected by the KOR selective agonist ICI-204,448. Two-tailed t test, n=13 mice for LPC and 5 for ICI-204,448.

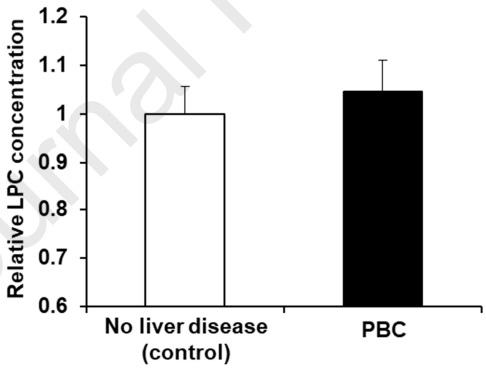

Supplementary Figure. 13. There was no significant difference in systemic LPC levels between patients in a gastroenterology-hepatology outpatients clinics not having liver disease, as indicated by normal liver histology, referred to as "control" vs PBC patients, the latter with unknown itch/no-itch status. Two-tailed t test, n=35 for control patients and n=25 for PBC patients, both cohorts recruited via the Duke Gastroenterology-Hepatology outpatient program, non-alcoholic fatty liver disease (NAFLD) clinical research program.

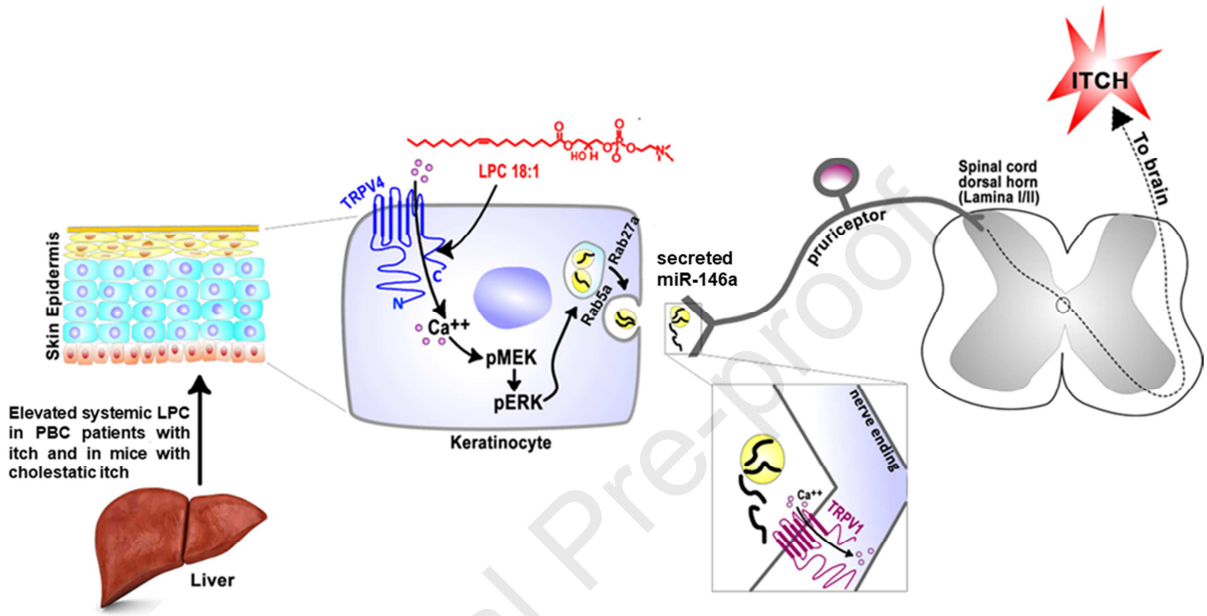

Supplementary Figure 14. Schematic diagram depicting the potential mechanism underlying cholestatic itch.

Cholestatic liver disease is associated with significantly elevated systemic LPC, which directly activates TRPV4 expressed in skin keratinocytes. This in turn leads to extracellular release of miR-146a via MEK-ERK-Rab5a/Rab27a signaling pathways. miR-146a functions as a pruritogen by activating TRPV1-expressing pruriceptor sensory neurons that innervate the skin. Activation of TRPV1 by miR-146a induces the sensation of itch via central pathways.

Supplementary Movie 1. 3D structural rendering of TRPV4 tetramer with the green subunit binding of LPC 18:1.

Supplementary Movie 2. *Ex vivo* imaging of DRG explants illustrating live Ca^{2+} signal of $GCaMP3^{+}$ sensory neurons in response to miR-146a (300nM) and capsaicin (1μM).